ChemPubSoc Europe

DOI: 10.1002/chem.201304153

CHEMISTRY A European Journal Full Paper

Supramolecular Chemistry | *Very Important Paper*

VIP Supramolecular ssDNA Templated Porphyrin and Metalloporphyrin Nanoassemblies with Tunable Helicity

Gevorg Sargsyan, Brian M. Leonard, Jan Kubelka, and Milan Balaz*[a]

Dedicated to Professor Arlette Solladié-Cavallo and Professor Marta Salisova

Abstract: Free-base and nickel porphyrin–diaminopurine conjugates were formed by hydrogen-bond directed assembly on single-stranded oligothymidine templates of different lengths into helical multiporphyrin nanoassemblies with highly modular structural and chiroptical properties. Large red-shifts of the Soret band in the UV/Vis spectroscopy confirmed strong electronic coupling among assembled porphyrin–diaminopurine units. Slow annealing rates yielded preferentially right-handed nanostructures, whereas fast annealing yielded left-handed nanostructures. Time-dependent DFT simulations of UV/Vis and CD spectra for model porphyrin clusters templated on the canonical B-DNA and its enantiomeric form, were employed to confirm the origin of observed chiroptical properties and to assign the helicity of porphyrin nanoassemblies. Molar CD and CD anisotropy g factors of dialyzed templated porphyrin nanoassemblies showed very high chiroptical anisotropy. The DNA-templated porphyrin nanoassemblies displayed high thermal and pH stability. The structure and handedness of all assemblies was preserved at temperatures up to $+85\,^{\circ}C$ and pH between 3 and 12. High-resolution transition electron microscopy confirmed formation of DNA-templated nickel(II) porphyrin nanoassemblies and their self-assembly into helical fibrils with micrometer lengths.

Introduction

Chiroptical organic and inorganic nanomaterials have great potential for applications in chiral memory, data storage, biological sensing, and optical communication.[1] Modulation of their chiroptical properties can be achieved by inverting the structure of chiral structural units or by changing the 3D structure of a chiral supramolecular nanoassembly by means of external stimuli. The latter approach brings several advantages originating from cooperativity and enhanced optical and chiroptical properties of nanoassemblies in comparison to single chiral molecules. Porphyrins and their derivatives are among the most-employed building blocks in organic nanoassemblies owing to their well-developed chemistry, stability, and modular structural and photophysical properties.[2] Optically active supramolecular multiporphyrin nanoassemblies of both helicities have previously been prepared through directional stirring,[3] by rotational forces and magnetic levitation,[4] and by directional templated assembly.[5] However, only the last approach allows controlling the helicity together with the size of nanoassemblies, thus controlling their structural and photophysical properties. Short DNA sequences gained prominence in templated bottom-up nanofabrication of multichromophoric supramolecular polymers owing to their versatile structural properties.[6] Combination of hydrogen bonding molecular recognition (nucleobase complementarity) and π–π stacking controls the architecture and characteristics of nanostructures.[7]

We have recently shown that porphyrin–diaminopurine conjugate 2HPor-DAP (Scheme 1) could be successfully assembled along single stranded oligothymidine (5′-dT40) into right- and left-handed helical nanostructures by directional hydrogen bonding.[5] The helicity and chiroptical properties of nanoassemblies was modulated by ionic strength and annealing rate. Herein, we explored formation of DNA-templated porphyrin nanoassemblies using 1) oligothymidine templates of different length (5′-dT8, 5′-dT16 and 5′-dT40) and 2) free-base porphyrin (2HPor-DAP), nickel(II)porphyrin (NiPor-DAP), and zinc(II)-porphyrin (ZnPor-DAP). Nickel and zinc porphyrins have been selected to evaluate the influence of metalation and axial ligands on formation of templated porphyrin nanoassemblies. Zinc porphyrins are five-coordinate, while nickel porphyrins are four- and six-coordinate in aqueous solutions with water as (an) axial ligand(s).[8] The DNA templated multiporphyrin nanoassemblies exhibited modular structural and chiroptical properties and high thermal stability. We have constructed molecular models for the 2HPor-DAP nanoassemblies and employed time-dependent density functional theory (TDDFT) simulations of UV/Vis and CD spectra for direct comparison with experimental data. The good qualitative agreement of the simulations with the experimental CD patterns confirmed the origin of observed CD profiles and helped to assign the helicity of

[a] *G. Sargsyan, Prof. B. M. Leonard, Prof. J. Kubelka, Prof. M. Balaz*
Department of Chemistry, University of Wyoming
1000 E. University Avenue, Laramie, WY 82071 (USA)
Fax: (+1) 307-766-2807
E-mail: mbalaz@uwyo.edu

Supporting information for this article is available on the WWW under http://dx.doi.org/10.1002/chem.201304153.

© 2014 Wiley-VCH Verlag GmbH & Co. KGaA, Weinheim

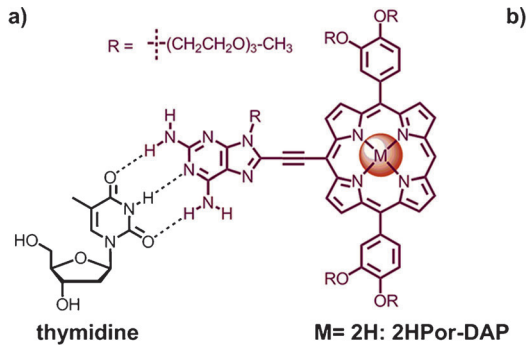

Scheme 1. a) Hydrogen bonding between porphyrin–diaminopurine conjugate 2HPor-DAP and thymidine. b) Representation of right-handed DNA-templated multiporphyrin nanoassembly.

optically active multiporphyrin nanoassemblies. High-resolution transmission electron microscopy (HRTEM) has shown formation of DNA-templated nanoassemblies and their self-assembly into fibril structures.

Results and Discussion

Synthesis of porphyrin–diaminopurine conjugates 2HPor-DAP, NiPor-DAP, and ZnPor-DAP

Diaminopurine–acetylene conjugate **4** was prepared in four steps from commercially available 2,6-diaminopurine (Scheme 2). The 2,6-diaminopurine DAP was deprotonated by NaH and reacted with triethylene glycol monomethyl ether tosylate. N-triethyleneglycol–diaminopurine **1** was then brominated by dropwise addition of NBS solution in acetonitrile over 1 h. The brominated diaminopurine **3** was reacted with mono(trihexylsilane)acetylene under Sonogashira cross-coupling reaction conditions to yield the trihexylsilane-protected diaminopurine–acetylene conjugate **3**. The trihexylsilane protection group was removed with TBAF to give the diaminopurine–acetylene conjugate **4**. Bis(triethyleneglycol)-substituted 3,4-dihydroxy-benzaldehyde **5** was prepared according to a previously reported procedure.[9] The 5,15-bisaryl-porphyrin **6** was prepared by Lindsey's acid-catalyzed condensation of dipyrromethane with aldehyde **5**, followed by oxidation with DDQ. Metalation with zinc acetate yielded zinc(II) porphyrin **7**. The bromination of **7** with NBS in chloroform and pyridine followed by separation yielded the monobrominated porphyrin **8**. Coupling of **8** and diaminopurine–acetylene **4** under Sonogashira cross-coupling conditions gave the diaminopurine–porphyrin conjugate ZnPor-DAP. The 2HPor-DAP was prepared by demetalation of ZnPor-DAP using TFA. Ni-derivative NiPor-DAP was prepared by refluxing the 2HPor-DAP with nickel acetate in DMF. The structures of porphyrin–diaminopurines conjugates were confirmed by ^{1}H NMR (Supporting Information, Figures S1, S2) and MALTI-TOF mass spectrometry.

Assembly of right-handed 2HPor-DAP:dTx and NiPor-DAP:dTx nanoassemblies by slow annealing

Slow annealing of 2HPor-DAP with dT40 in the presence of 500 mM NaCl resulted in preferential formation of right-handed 2HPor-DAP:dT40 helix (see section *Theoretical simulations of CD spectra* for the helicity assignment). The CD spectrum showed a positive CD band at 423.0 nm (+52.7 mdeg) and two negative CD bands at 379.3 nm (−10.5 mdeg) and 495.6 nm (−29.1 mdeg) in the Soret band region (Figure 1a). Negative CD bands at 609.6 nm (−16.1 mdeg) and 684.5 nm (−12.9 mdeg) were detected in the Q-band region. Strong CD signals are consistent with formation of helical nanostacks of 2HPor-DAP conjugates along an oligothymine template.

Similarly, dT16 successfully templated formation of the *P*-isomer of 2HPor-DAP:dT16 with a positive Cotton effect at 427.1 (+51.2 mdeg) and two negative CD bands at 379.3 nm (−10.5 mdeg) and 496.6 nm (−17.1 mdeg) in the Soret band

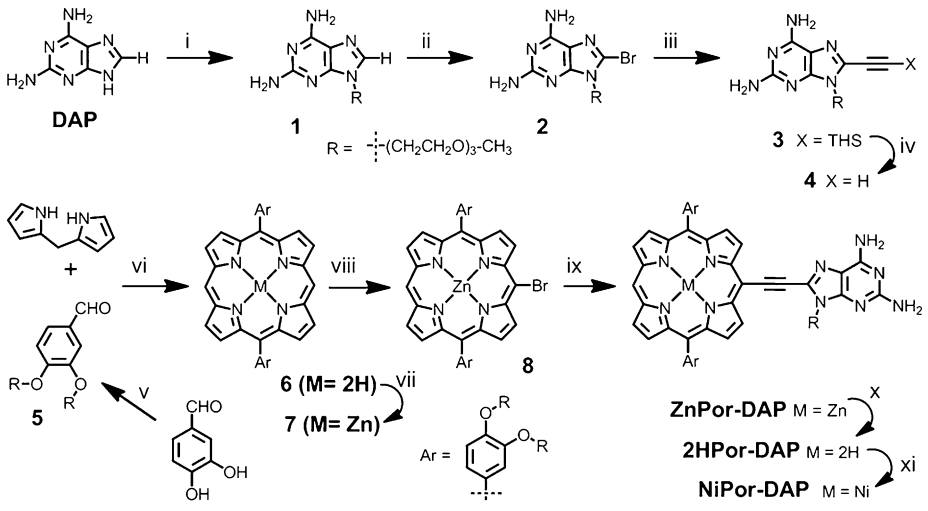

Scheme 2. Synthesis of porphyrin–diaminopurine conjugates 2HPor-DAP, NiPor-DAP, and ZnPor-DAP. i) 1) NaH, DMF, 60 °C, 2 h; 2) 2-(2-(2-methoxyethoxy)ethoxy)ethyl 4-methylbenzenesulfonate, 0 °C, 7 h; ii) *N*-bromosuccinimide (NBS), CH_3CN, RT, 1.5 h; iii) $[Pd_2(dba)_3]$, Ph_3P, (*n*hex)$_3$Si–C≡CH, CuI, piperidine, 40 °C, 4 h; iv) tetra-*n*-butylammonium fluoride (TBAF), CH_2Cl_2, RT, 30 min; v) triethylene glycol monomethyl ether tosylate, K_2CO_3, CH_3CN; vi) trifluoroacetic acid (TFA), then 2,3-dichloro-5,6-dicyano-1,4-benzoquinone (DDQ); vii) $Zn(OAc)_2{\cdot}2H_2O$, $CHCl_3$, CH_3OH, RT; viii) NBS, $CHCl_3$, C_5H_5N; ix) **4**, $[Pd_2(dba)_3]$, Ph_3P, CuI, DMF, triethylamine (TEA), 40 °C, 15 h; x) TFA, CH_2Cl_2, RT, 4 h; xi) $Ni(OAc)_2{\cdot}4H_2O$, DMF, 120 °C, 4 h.

© 2014 Wiley-VCH Verlag GmbH & Co. KGaA, Weinheim

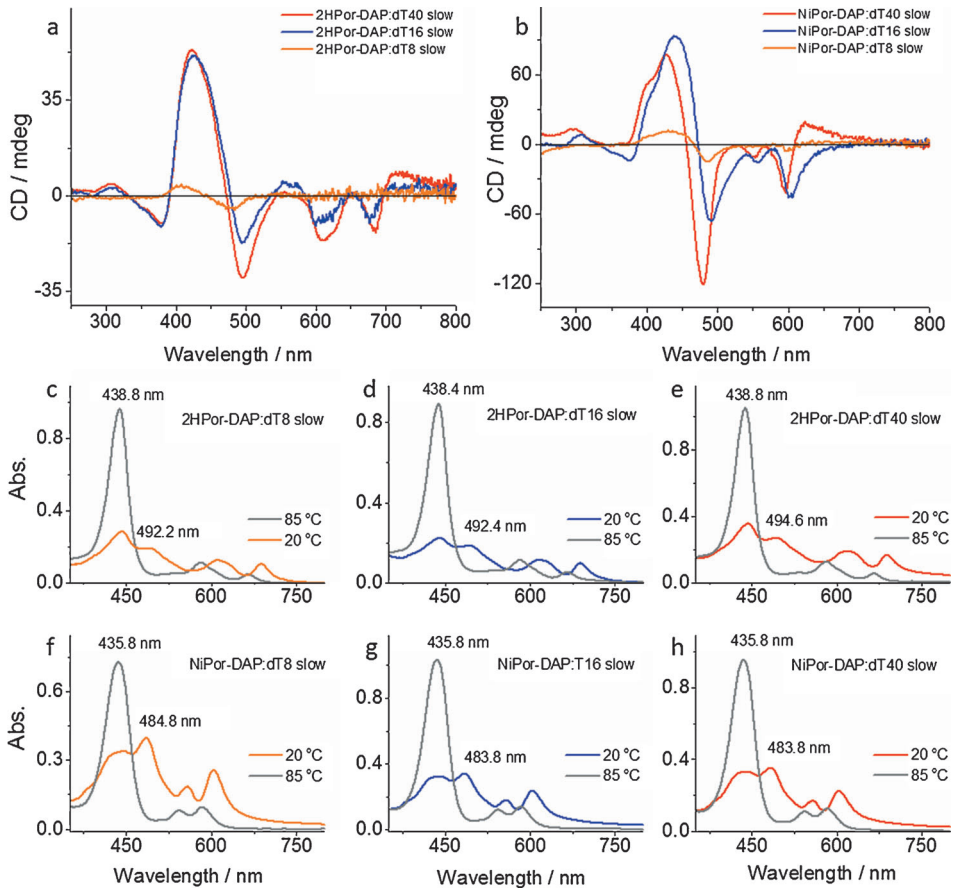

Figure 1. CD and UV/Vis spectra of right-handed oligothymidine-templated 2HPor-DAP:dTx and NiPor-DAP:dTx nanoassemblies prepared by slow annealing. 2HPor-DAP:dTx: slow annealing of 2HPor-DAP (10 μM) with dTx (10 μM) in 40% DMSO Na-cacodylate buffer (1 mM, pH 7.0, 500 mM NaCl (dT40) and 200 mM NaCl (dT16). NiPor-DAP:dTx: slow annealing of NiPor-DAP (10 μM) with dTx (10 μM) in 45% DMSO Na-cacodylate buffer (1 mM, pH 7.0, 100 mM NaCl.

region. Two additional negative Cotton effects were observed in the Q-band region at 605.0 nm (−9.5 mdeg) and 677.0 nm (−8.1 mdeg). Similar CD spectra for 2HPor-DAP:dT40 and 2HPor-DAP:dT16 suggested their similar structures. Annealing of 2HPor-DAP with the shortest template dT8 yielded a right-handed 2HPor-DAP:dT8 nanostructure characterized by a negative CD band at 477.7 nm (−4.4 mdeg) and a positive CD band at 409.85 nm (+3.97 mdeg). No CD bands were observed in the Q-band region.

Slow annealing of NiPor-DAP with dT40 in the presence of 100 mM NaCl also resulted in the assembly of preferentially right-handed NiPor-DAP:dT40 nanoarrays characterized by a negative Cotton effect 478.9 nm (−120 mdeg) and a positive Cotton effect at 426.0 nm (+75.0 mdeg) in the Soret band region (Figure 1b). Negative CD bands at 550 nm (−10.7 mdeg) and 595.2 nm (−40.7 mdeg) and a positive CD band at 620 nm (+20 mdeg) were detected in the Q-band region. The chiral right-handed assembly NiPor-DAP:dT16 was also successfully formed upon slow annealing of NiPor-DAP with the shorter dT16 template, as evidenced by a positive CD band at 440.6 nm (+93.3 mdeg) and a negative CD band at 491.0 nm (−63.9 mdeg) in the Soret region. Two negative Cotton effects were observed in the Q-band absorption region at 603.5 nm (−45.6 mdeg) and 557.2 nm (−15.4 mdeg). Similarly to 2HPor-DAP, NiPor-DAP assemblies formed by slow annealing on a dT8 template resulted in a weaker CD signal in the Soret absorption region with maxima at 435.1 nm (+12.9 mdeg) and 485.0 nm (−13.9 mdeg).

The formation of right-handed 2HPor-DAP:dTx ($x=8$, 16 and 40) and NiPor-DAP:dTx nanoassemblies by slow annealing caused large red-shifts of the Soret bands (up to 54.4 nm) and Q-bands (up to 33.4 nm) in the absorption spectra indicative of strong electronic coupling between porphyrin–diaminopurine chromophores (Figure 1c–1h and Table 1). The red-shifts suggested that porphyrin–diaminopurine conjugates adopted structures similar to J-aggregates within the DNA-templated multiporphyrin nanoassemblies.

The presence and type of transition metal in the porphyrin coordination center also influenced nanoassembly formation. Free-base and nickel porphyrins exhibited similar behavior while all attempts to prepare chiral dT40 templated nanoassemblies of ZnPor-DAP conjugate failed. We have unsuccessfully tested slow and fast annealing while varying the DMSO content from 1% to 70% in Na-cacodylate buffer (1 mM, pH 7.0) as well as increasing the ionic strength (up to 500 mM NaCl). Zinc porphyrins are five coordinate in aqueous solutions and have been shown not to lose the axial water ligand easily.[8] On the other hand, nickel porphyrins have been shown to easily lose axial ligands to form four-coordinate species.[10] We hypothesized that the axial ligand on the zinc atom sterically prevented the efficient π-stacking and hampered formation of ZnPor-

Table 1. Soret band and Q-band shifts upon annealing of porphyrin–diaminopurine conjugates with oligothymidine templates.

	2HPor-DAP:dTx ($\Delta_{Soret}/\Delta_{Q\text{-}band}$)[a]		NiPor-DAP:dTx ($\Delta_{Soret}/\Delta_{Q\text{-}band}$)[a]	
	slow annealing	fast annealing	slow annealing	fast annealing
dT40	54.4/33.4	47.2/28.0	47.6/20.6	42.2/16.8
dT16	52.8/30.9	42.4/26.6	49.0/20.6	45.0/18.2
dT8	50.4/28.2	47.2/28.2	49.2/20.4	47.2/19.2

[a] Soret band and Q-band bathochromic shifts [nm].

© 2014 Wiley-VCH Verlag GmbH & Co. KGaA, Weinheim

DAP:dT40 nanoassemblies. Similar behavior has been previously observed for zinc-porphyrin–DNA capping.[2d,11]

Helicity control of 2HPor-DAP:dTx and NiPor-DAP:dTx nanoassemblies: Fast annealing

We have shown previously that the handedness of the oligothymidine templated porphyrin–diaminopurine conjugate (2HPor-DAP:dT40) can be controlled and opposite helicities can be obtained by controlling the ionic strength and annealing rate of the precursors.[5] The slow annealing (linear cooling at 0.5 °C min^{-1}; cooling time from 85 °C to 20 °C = 260 min) in the presence of NaCl has been shown to form predominately right-handed nanoassemblies. On the other hand, the fast annealing (non-linear cooling; cooling time from 85 °C to 20 °C < 5 min) in the presence of NaCl provided predominantly left-handed nanostructures. We have therefore explored the effect of annealing rates on the helicity of assembled nanostructures while varying the oligothymidine lengths and metal in the coordination center of the porphyrin (free-base and nickel).

Fast annealing of 2HPor-DAP with dT40 in the presence of 100 mM NaCl resulted in preferential formation of left-handed 2HPor-DAP:dT40 nanoassemblies, characterized by a negative CD band at 461.6 nm (−57.7 mdeg) and positive CD bands at 400.1 nm (46.9 mdeg) and at 500.0 nm (+21.8 mdeg) in the Soret band region (Figure 2a, green curve). The Q-band absorption region revealed positive CD bands at 626.1 nm (+8.4 mdeg) and 693.5 nm (+7.8 mdeg) and a negative band at 598.1 nm (−4.0 mdeg). The shorter template dT16 also promoted formation of left-handed 2HPor-DAP:dT16, as indicated by appearance of a negative Cotton effect at 462.2 nm (−27.9 mdeg) and positive Cotton effects at 397.1 nm (+30.6 mdeg) and 497.3 nm (+19.7 mdeg) in the Soret region (Figure 2a, purple curve). The Q-band region displayed positive CD bands at 619.7 nm (+7.8 mdeg) and 682.5 nm (+7.1 mdeg). Shortest dT8 also promoted assembly of 2HPor-DAP, although with weaker CD signals in Soret region and no CD signal in the Q-band region (Figure 2a, cyan curve). Fast annealing of NiPor-DAP in the presence of oligothymidine templates promoted preferential formation of left-handed helices. (*M*)-NiPor-DAP:dT40 nanoassemblies displayed positive CD bands at 488.7 nm (43.0 mdeg) and 390.9 nm (23.2 mdeg) and a negative band at 462.2 nm (−75.7 mdeg) in the Soret region (Figure 2b, green curve). Positive Cotton effects at 602.8 nm (+15.9 mdeg) and 556.1 nm (+5.1 mdeg) and a negative Cotton effect at 587.3 nm (−6.4 mdeg) were observed in the Q-band region. Shorter NiPor-DAP:dT16 nanoassemblies exhibited a very similar CD profile to longer NiPor-DAP:dT40. The CD spectrum showed positive CD bands at 490.6 nm (+53.4 mdeg) and 392.3 nm (+31.9 mdeg) and a negative band 466.4 nm (−87.6 mdeg) in the Soret region (Figure 2b, purple curve). Positive Cotton effects at 604.8 nm (+23.0 mdeg) and at 557.2 nm (+5.6 mdeg) and a negative Cotton effect at 586.4 nm (−5.6 mdeg) were observed in the Q-band region. The dT8 sequence yielded a similar CD profile with smaller negative and positive CD signals at 468.4 nm (−5.3 mdeg) and 395.1 nm (+6.8 mdeg), respectively. Fast annealing of left-handed 2HPor-DAP:dTx and NiPor-DAP:dTx nanoassemblies resulted in large red-shifts of the Soret bands (up to 47.2 nm) and Q-bands (up to 28.2 nm) in the absorption spectra (Figure 2c–h and Table 1). Fast annealing yielded nanoassemblies with smaller red-shifts than those formed by slow annealing. Similarly, 2HPor-DAP:dTx exhibited larger red-shifts of the Soret and Q-bands than the nickel derivatives indicating differences in angles and distances

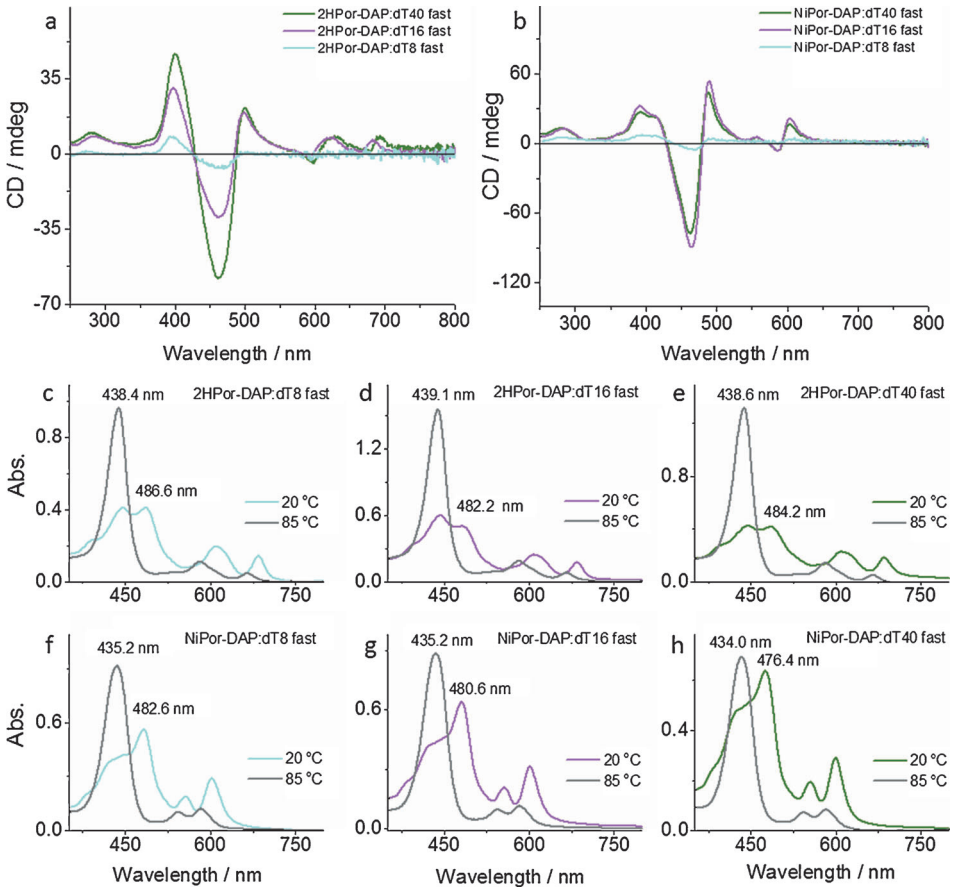

Figure 2. CD and UV/Vis spectra of left-handed oligothymidine-templated 2HPor-DAP:dTx and NiPor-DAP:dTx nanoassemblies prepared by fast annealing. Conditions: [MPor-DAP] = 10 μM (M = 2H or Ni), [dTx] = 10 μM, 40% DMSO Na-cacodylate buffer (1 mM, pH 7.0, 100 mM NaCl).

© 2014 Wiley-VCH Verlag GmbH & Co. KGaA, Weinheim

between porphyrin–diaminopurine conjugates in right- and left-handed nanoassemblies.

All three of the oligothymidine templates successfully assembled 2HPor-DAP and NiPor-DAP conjugates into chiral nanostacks under both annealing rates. The length of the template and the annealing rate had a pronounced effect on the CD signature of assembled nanostructures. The longest oligothymidine template, dT40, provided the most intense CD spectra under slow as well as fast annealing conditions for 2HPor-DAP and NiPor-DAP. The nanoassemblies formed along the shortest template, dT8, gave rise to weaker CD spectra with a slightly different CD profile than their longer counterparts. The annealing rate controlled the helicity of formed nanoassemblies with slow annealing yielding preferentially right-handed assemblies (*P*-helix) and the fast annealing yielded favorably the left-handed assemblies (*M*-helix) when using dT40 and dT16 oligothymidine templates (Figure 3). The *M*-isomers of the 2HPor-DAP:dT40 and 2HPor-DAP:dT16 nanoassemblies, *P*-isomers of 2HPor-DAP:dT40 and 2HPor-DAP:dT16 nanoassemblies, and *M*-isomers of the NiPor-DAP:dT40 and NiPor-DAP:dT16 nanoassemblies, had very similar CD signatures for each pair, which differed only in their intensities. The CD spectroscopic data suggested that the dT8 template does not allow both helicities to be successfully accessed.

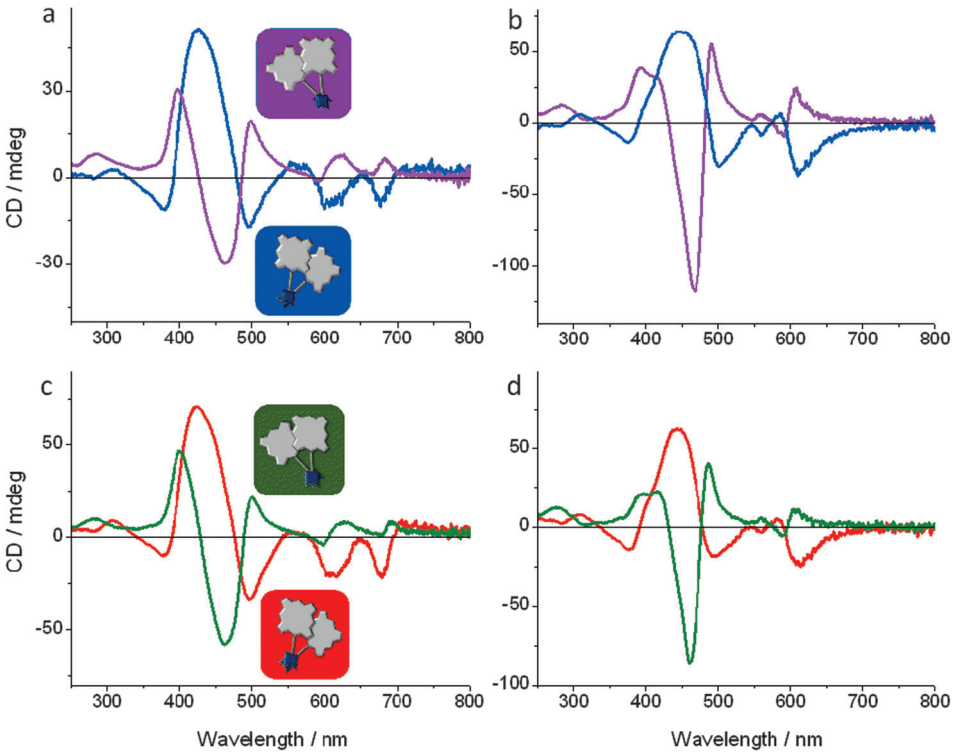

Figure 3. Comparison of CD spectra of right-handed and left-handed a) 2HPor-DAP:dT16 nanoassemblies, b) NiPor-DAP:dT16 nanoassemblies, c) 2HPor-DAP:dT40, and d) NiPor-DAP:dT40 nanoassemblies, prepared by slow (red) and fast (green) annealing. Slow annealing of 2HPor-DAP (10 μM) with dT16 (10 μM) in 40% DMSO, Na-cacodylate buffer (1 mM, pH 7.0, 200 mM NaCl). Fast annealing of 2HPor-DAP (10 μM) with dT16 (10 μM) in 45% DMSO, Na-cacodylate buffer (1 mM, pH 7.0, 100 mM NaCl). Slow and fast annealing of NiPor-DAP (10 μM) with dTx (10 μM) in 40% DMSO, Na-cacodylate buffer (1 mM, pH 7.0, 100 mM NaCl).

Theoretical simulations of CD spectra

Theoretical simulations of UV/Vis and CD spectra for model porphyrin assemblies[5] were carried out using the Gaussian 09 program.[12] The model structures were constructed from a 2HPor-DAP monomer whose geometry was fully optimized at B3LYP/6-31G(d,p) level of theory. The right-handed 2HPor-DAP assemblies (*P*-helix) were formed by attachment of the individual 2HPor-DAP conjugates to the poly(dT) DNA strand in a B-form, to form canonical (Watson–Crick) hydrogen bonds. This resulted in the vertical distance and angle between the successive 2HPor-DAP units of 3 Å and 34°, respectively. Supramolecular 2HPor-DAP oligomers of two to six units were built. The left-handed structures were obtained simply by inverting the angle of the neighboring 2HPor-DAP conjugates (−34°). The 2HPor structures were obtained from 2HPor-DAP by deleting the diaminopurine. A model structure for the *P*-helix of the 2HPor-DAP tetramer is depicted in Figure 4a. Excited-state calculations were carried out at time-dependent density functional theory (TDDFT) level, using a B3LYP hybrid functional. Dipolar and rotational strengths were computed using both dipole-length and dipole-velocity gauge formalisms and found to be essentially identical; only dipole-velocity results are presented. The computed rotational strengths were converted to molar extinction coefficients and convoluted with Gaussian band shapes of a uniform half-width of 25 nm. Owing to the size of the model systems, along with the large number of excited states (>500) that has to be computed to adequately represent the CD spectra, small basis sets are necessary to keep the calculations tractable. Basis-set dependence was tested on 2HPor dimers, as shown in Figure 4b. Larger basis sets resulted in a red-shift on the spectrum along with an increase of the CD intensity, but the overall sign pattern and shape of the CD were essentially independent of the basis set. Furthermore, the effect of solvent (water) on the computed spectra was tested using conductor-like polarized continuum model (CPCM) as implemented in Gaussian 09 (Supporting Information, Figure S3). Including implicit solvent likewise resulted in a slight red-shift of the spectrum, but it only had a minor effect on the CD.

The CD spectra calculated for the model *P*- and *M*-helix structures are shown in Figure 4c. The simulations were carried out for 2HPor-DAP tetramers using the TD B3LYP/3-21G level of theory. The predicted CD patterns in the Soret region (com-

© 2014 Wiley-VCH Verlag GmbH & Co. KGaA, Weinheim

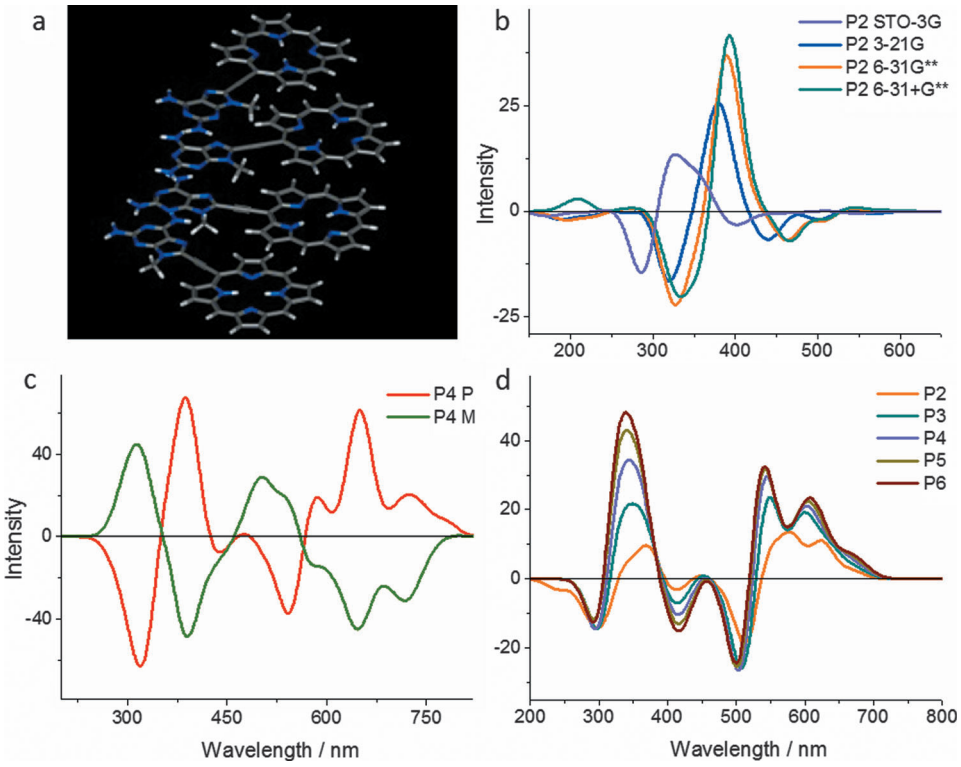

Figure 4. a) 2HPor-DAP model structure for the *P*-helix. Comparison of simulated (B3LYP/3-21G) CD spectra for model *P*-helix (red) and *M*-helix (green) structures of 2HPor-DAP tetramer. b) Dependence of the simulated (B3LYP/STO-3G) CD spectra on the number of 2HPor-DAP units stacked in the *P*-helix model structure. c) TD-DFT simulations of CD spectra for model porphyrin nanoassemblies (from dimer to hexamer). Intensities are normalized to a single 2HPor unit. d) Basis set dependence of the CD spectra simulated with B3LYP density functional for the *P*-helix 2HPor dimer.

puted between 250–450 nm) are in a good qualitative agreement with the experimental data (compare to Figure 3a,c). An intense negative couplet predicted for the model *M*-helix is seen experimentally. However, essentially an oppositely signed couplet is predicted for the *P*-helix with only a small additional negative CD on the short wavelength side, while experimental data show a distinct −/+/− pattern. This suggests that the model structures, in particular of the *P*-helix, may not be accurate. The model structures are likely also responsible, at least in part, for a too high CD signal computed at longer wavelengths (500–800 nm) in 2HPor-DAP models, which is not seen experimentally. Close stacking of DAP rings (Figure 4a) overemphasizes their contributions to the spectra over that of the 2HPor. As the calculations are necessarily limited to small number of stacked rings, another possible source of discrepancy between the experiment and simulations may be the size of the stacked assembly. The dependence of the CD on the number of stacked 2HPor-DAP was tested at TD-B3LYP/STO-3G level (Figure 4d). These simulations show that the Soret band CD intensity does grow more significantly with the assembly size than do the 500–800 nm signals, and that relative intensity of the negative CD to the red of the main couplet increases. Both these trends are in the direction of experimental *P*-helix CD.

All combined, considering the limitation of the theoretical simulations particularly in regard to size, the simulations reproduced the experimentally observed CD very well. All tests of the necessary approximations, such as the neglect of solvent (Supporting Information, Figure S3), small basis sets, and limitation to a small number of 2HPor-DAP units (Figure 4), showed correct trends toward better correspondence with the experiment. While further work is necessary to determine the definite structural arrangements adopted by these nanoassemblies, the structures based on *M*- and *P*-helices are very reasonable models.

Dialysis: Purification of porphyrin–diaminopurine nanoassemblies 2HPor-DAP:dT40 and NiPor-DAP:dT40

To characterize the structural and photophysical properties of DNA-templated porphyrin nanoassemblies, we separated them from porphyrin monomers. We used dialysis (2kDa cassettes), a widely used technique for removal of small contaminants from macromolecular systems. Dialysis allowed us to remove non-assembled porphyrin conjugates together with the DMSO and NaCl. The DMSO concentration was decreased from 40% to 0.0028%, whereas the NaCl concentration was decreased from 100 mM to 0.007 mM. The dialyzed 2HPor-DAP:dT40 solution was characterized by UV/Vis absorption, emission, and CD spectroscopy. The absorption spectrum displayed a maximum at 491.0 nm with a shoulder at about 435 nm (Figure 5c, blue curve). The intensity of 440.0 nm absorption band corresponding to non-assembled 2HPor-DAP conjugates notably decreased. A CD spectrum of dialyzed 2HPor-DAP:dT40 revealed an identical profile with reduced intensity in comparison to the pre-dialysis sample (Figure 5a). CD spectrum confirmed the presence of chiral right-handed 2HPor-DAP:dT40 nanoassemblies after dialysis.

Emission spectra of dialyzed 2HPor-DAP:dT40 displayed a single emission band at 685 nm, which was independent of excitation wavelength (483.0 nm or 438.0 nm; Figure 5e). UV/Vis absorption and emission spectra confirmed that dialysis successfully removed the non-assembled 2HPor-DAP units from the 2HPor-DAP:dT40 nanoassemblies. NiPor-DAP:dT40 was dialyzed using the same procedure as 2HPor-DAP:dT40. The dialyzed solution was characterized by UV/Vis absorption and CD spectroscopy. The absorption spectrum displayed a maximum at 482.8 nm with a shoulder at about 420 nm (Figure 5d, blue curve). The 438.0 nm absorption band present in

© 2014 Wiley-VCH Verlag GmbH & Co. KGaA, Weinheim

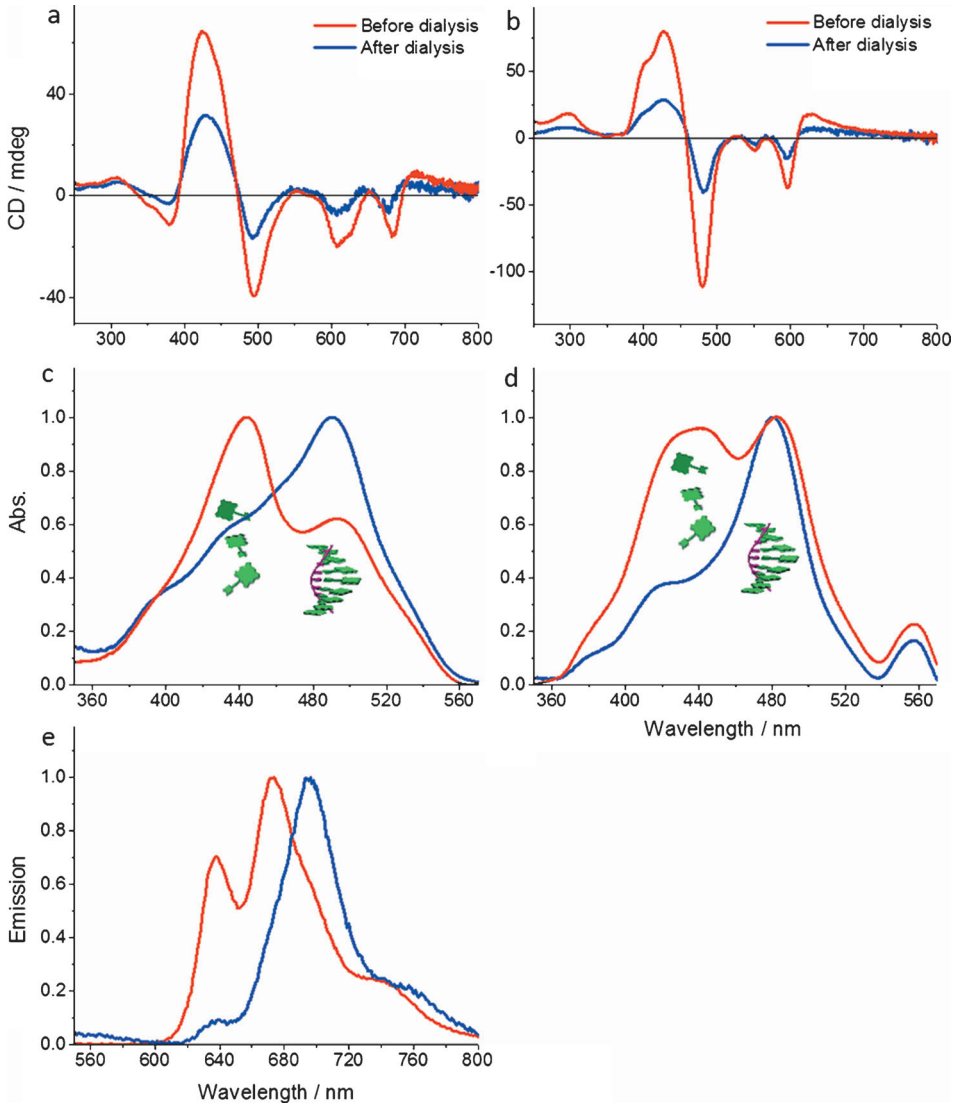

Figure 5. a), b) CD, c), d) normalized UV/Vis absorption, and e) normalized emission spectra of 2HPor-DAP:dT40 (left column) and NiPor-DAP:dT40 (right column) before dialysis (red) and after dialysis (blue). Nanoassemblies were prepared by slow annealing in Na-cacodylate buffer (1 mM, pH 7.0). 2HPor-DAP:dT40 (40% DMSO, 500 mM NaCl), NiPor-DAP:dT40, (45% DMSO, 100 mM NaCl).

the spectrum of the NiPor-DAP:dT40 assembly before dialysis significantly diminished. Dialysis therefore successfully removed the non-assembled NiPor-DAP conjugates from the helical NiPor-DAP:dT40 nanoassembly. CD spectrum of the dialyzed NiPor-DAP:dT40 solution revealed identical features, with a reduced intensity in comparison to the pre-dialysis sample (Figure 5b). A CD spectrum confirmed the presence of chiral NiPor-DAP:dT40 nanoassemblies after dialysis. Similar results have been observed for the dialysis of left-handed 2HPor-DAP:dT40 and NiPor-DAP:dT40 prepared by fast annealing and right- and let-handed handed 2HPor-DAP:dT16 and NiPor-DAP:dT16 nanoassemblies prepared by slow and fast annealing, respectively (Supporting Information, Figures S5–S7).

Molar CD and CD anisotropy of porphyrin nanoassemblies

After purifying the 2HPor-DAP:dTx and NiPor-DAP:dTx nanoassemblies by dialysis, the concentrations of 2HPor-DAP and NiPor-DAP conjugates in the nanoassembly solutions were determined by melting the nanoassemblies by addition of DMSO and subsequent heating to 85 °C (see the Supporting Information). The Soret band absorption was then compared with the absorption of DNA-free porphyrin conjugates with known extinction coefficients under identical conditions. In a typical dialysis experiment, the concentration of porphyrin–diaminopurine conjugate was decreased from 10 μM to 3.0 μM. Knowing the concentrations of the porphyrins, the CD ellipticities (in millidegrees) were then converted into molar CD ($\Delta\varepsilon$, $L\,mol^{-1}\,cm^{-1}$), which allowed us to compare CD spectra of the different nanoassemblies at different concentrations. Molar CD spectra of dialysis purified 2HPor-DAP:dTx and NiPor-DAP:dTx nanoassemblies are plotted in Figure 6.

Slow annealing and longer oligothymidine template dT40 produced chiral nanostructures with stronger molar CD than fast annealing and shorter templates (dT16, dT8). Right-handed 2HPor-DAP:dT40 nanoassemblies prepared by slow annealing displayed one of the highest reported molar CD values per assembly unit in supramolecular structures ($\varepsilon = +$ 850 $L\,mol^{-1}\,cm^{-1}$ at 428.0 nm). Molar CD confirmed very efficient and strong chiral coupling between helically arranged 2HPor-DAP and NiPor-DAP conjugates.

To further evaluate the chiroptical characteristics of the nanoassemblies, their CD anisotropy factors (also referred as CD dissymmetry or g-factor) in the Soret band region were calculated. The CD anisotropy factor is defined as $g = \Delta\varepsilon/\varepsilon = (A_L - A_R)/A$, where A represents the conventional absorbance of non-polarized light and A_L and A_R are the absorptions of left and right circularly polarized light, respectively. The CD anisotropy factor is independent of the concentration and of the path length if the CD and absorbance spectra are taken on the same sample. Large anisotropy factors of up to 8.5×10^{-3} for

© 2014 Wiley-VCH Verlag GmbH & Co. KGaA, Weinheim

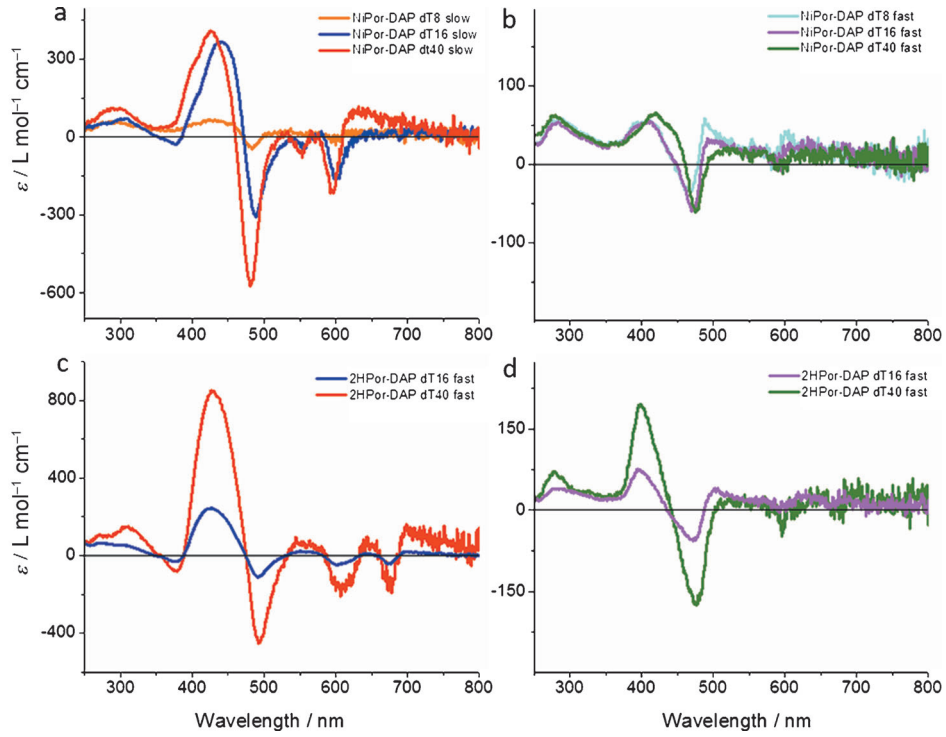

Figure 6. Molar CD spectra of a), b) NiPor-DAP:dTx and c), d) 2HPor-DAP:dTx nanoassemblies prepared by slow cooling (left column) and fast cooling (right column).

Table 2. CD anisotropy factors of porphyrin nanoassemblies prepared by slow and fast annealing measured for CD Cotton effects in the Soret band region.

	2HPor-DAP:dTx		NiPor-DAP:dTx	
dTx template	slow[a]	fast[a]	slow[a]	fast[a]
dT40	$+8.5\times10^{-3}$ (428.0 nm)	$+4.7\times10^{-3}$ (398.0 nm)	-6.7×10^{-3} (481.0 nm)	$+1.4\times10^{-3}$ (418.0 nm)
dT16	$+8.0\times10^{-3}$ (427.2 nm)	$+1.17\times10^{-3}$ (392.6 nm)	$+10.0\times10^{-3}$ (438.0 nm)	-0.7×10^{-3} (471.0 nm)

[a] Annealing rate of porphyrin nanoassembly preparation.[5]

right-handed 2HPor-DAP:dT40 and $g=10\times10^{-3}$ for right-handed NiPor-DAP:dT16 further confirmed intense dissymmetry of the DNA-templated multi-porphyrin nanoassemblies (Table 2).

HRTEM microscopy of dialyzed right-handed NiPor-DAP:dT40 nanoassemblies

To further investigate the DNA-templated porphyrin nanoassemblies, we have utilized high-resolution transmission electron microscopy (HRTEM) and high-angle annular dark-field imaging (HAADF). Figure 7 shows representative TEM micrographs of drop-casted dialyzed aqueous solutions of NiPor-DAP:dT40. Nanowires and helical fibrils with lengths from a few hundred nanometers to several micrometers have been observed. A detailed analysis of individual one-dimensional nanowires showed that the widths of the nanowires varied between 15 to 16 nm (Figure 7b; Supporting Information, Figure S4). These dimensions are in good agreement with the length predicted by the molecular model of NiPor-DA P:dT40 nanoassembly based on a B-DNA geometry (40 base pairs: length 13.2 nm). It is reasonable to assume that triethyleneglycol (TEG) chains (five TEG chains per each porphyrin–diaminopurine unit) promoted side-to-side interactions between NiPor-DAP:dT40 nanoassemblies and mediated the formation of supramolecular polymeric nanowires. A molecular representation of the NiPor-DAP:dT40 nanoassembly and its side-by-side assembly into a nanowire are demonstrated in Figure 7c. The nanowires were further elongated into helical polymeric

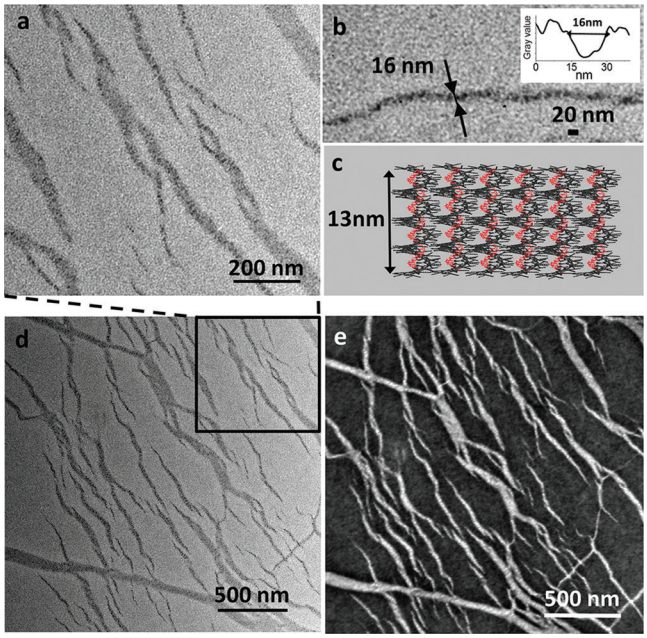

Figure 7. Bright field (a,b,d) and dark field (e) TEM images of right-handed NiPor-DAP:dT40 nanoassemblies. b) Inset: grey scale cross-section of the nanowire. c) Model representation of NiPor-DAP:dT40 nanoassembly and its side-to-side self-assembly into a nanowire. dT40 (red), NiPor-DAP (black).

fibrils. Helical twisting of wires around each other can clearly be seen in Figure 7a. The presence of nickel (II) in the coordination center of the porphyrin allowed us to study the nanowires using the HAADF mode, which is highly sensitive to

© 2014 Wiley-VCH Verlag GmbH & Co. KGaA, Weinheim

changes in atomic number. Dark-field imaging confirmed that all of the nanowires contained nickel atoms (Figure 7e), which are visible as bright areas compared to the carbon background. TEM studies thus confirmed the formation of NiPor-DAP:dT40 nanoassemblies and showed their self-assembly into helical fibrils of micrometer lengths.

Thermal and acid–base stability of Por-DAP:dT40 porphyrin nanoassemblies

Next we explored the influence of temperature and pH on the stability, spectroscopic, and conformational behavior of the of the dialyzed and non-dialyzed right- and left-handed DNA-templated 2HPor-DAP:dT40 and NiPor-DAP:dT40 porphyrin nanoassemblies. The structural stability of supramolecular nanoassemblies is one of key features for their future applications in nanomaterials. Because of relatively weak interactions, such as π–π stacking and hydrogen bonding, stability formation of functional supramolecular architectures with well-controlled morphology remains a challenge. Thermal stability was evaluated by heating a solution of dialyzed nanoassemblies in Na-cacodylate buffer (1 mM, pH 7.0) and also by heating a solution of non-dialyzed nanoassemblies in 40% DMSO, Na-cacodylate buffer (1 mM, pH 7.0 500 mM NaCl). The dialyzed right-handed 2HPor-DAP:dT40 nanoassemblies displayed a very high level of thermal stability and the nanoassemblies did not melt even at 85 °C (Figure 8). The shape of the CD spectrum did not change, although the CD intensity decreased. The 2HPor-DAP:dT40 thus remained in the helical structure after heating from 20 °C to 85 °C (Figure 8b). For comparison, Stulz and co-workers reported the complete disassembly of zipper porphyrin–DNA nanoassemblies with porphyrins covalently attached to two complementary DNA strands with temperatures of above 70 °C.[2c] Absorption spectra revealed a decrease of the shoulder at 430 nm without a shift of the λ_{max} (488 nm), while the emission spectra stayed virtually identical upon heating to 85 °C (Figure 8d,f).

Importantly, the 2HPor-DAP:dT40 remained a right-handed helical structure, with CD features similar to the original freshly prepared nanoassembly (Figure 1a) after five heating–cooling cycles (cycle: 20 °C→85 °C→20 °C; Figure 8b, dashed curve). On the other hand, heating the non-dialyzed right-handed 2HPor-DAP:dT40 nanoassembly from 20 °C to 85 °C caused its complete melting, as evidenced by CD, UV/Vis absorption, and emission spectra (Figure 8a,c,e). The CD signal completely disappeared for temperatures above 70 °C. Sigmoidal fit of the change of the 440 nm CD signal as a function of temperature allowed us to calculate the melting temperature T_m as 53.7 °C. At 85 °C, the absorption spectrum showed a disappearance of the 500 nm band, while the emission spectrum was altered into a single band at 700 nm.

Similarly to its free-base counterpart, the dialyzed right-handed NiPor-DAP:dT40 nanoassembly displayed very high

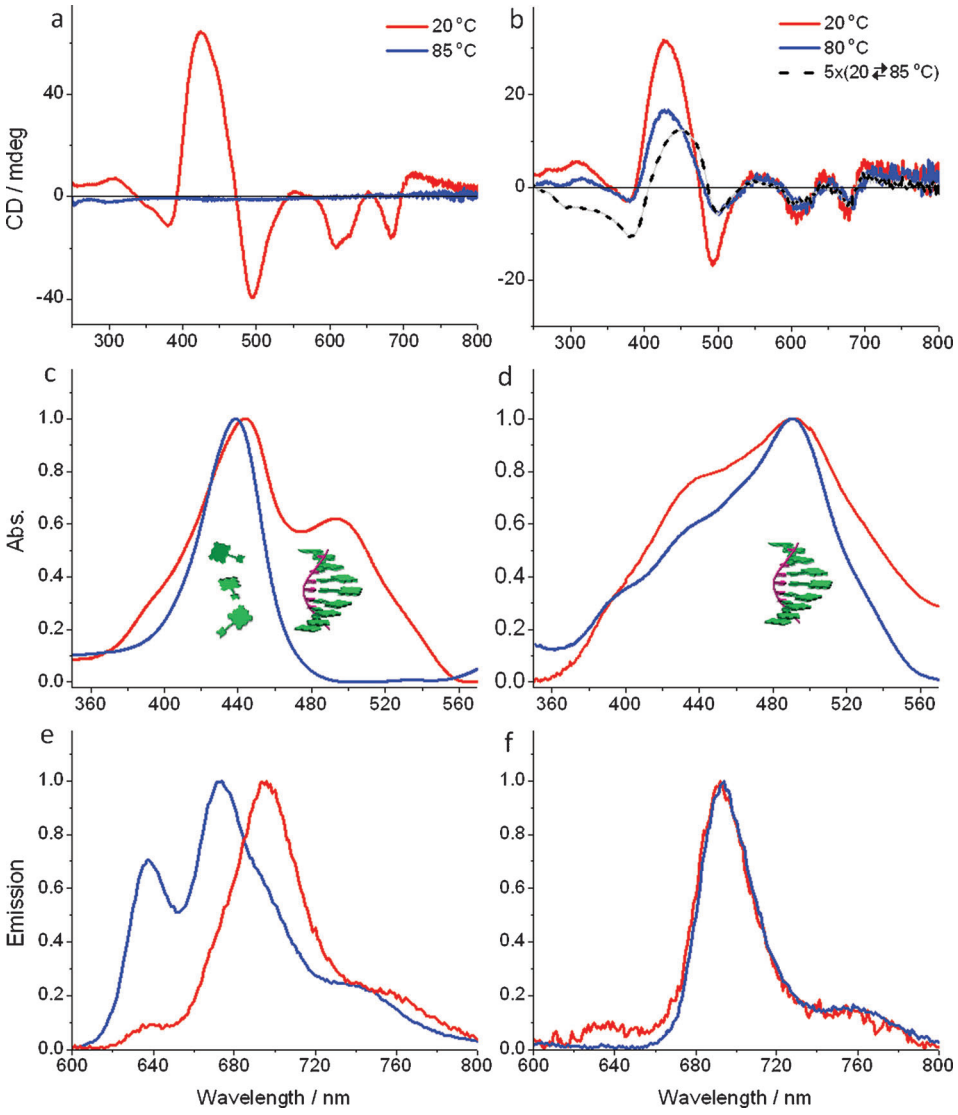

Figure 8. Variable-temperature a),b) CD, c),d) normalized UV/Vis absorption, and e),f) normalized emission spectra of the right-handed 2HPor-DAP:dT40 nanoassembly before dialysis (left spectra) and after dialysis (right spectra) at 20 °C (red), 85 °C (blue), and after five heating–cooling cycles (dashed curve). Assembly formation: [2HPor-DAP] = [dT40] = 10 μM; slow annealing in 40% DMSO Na-cacodylate buffer (1 mM, pH 7.0, 500 mM NaCl).

© 2014 Wiley-VCH Verlag GmbH & Co. KGaA, Weinheim

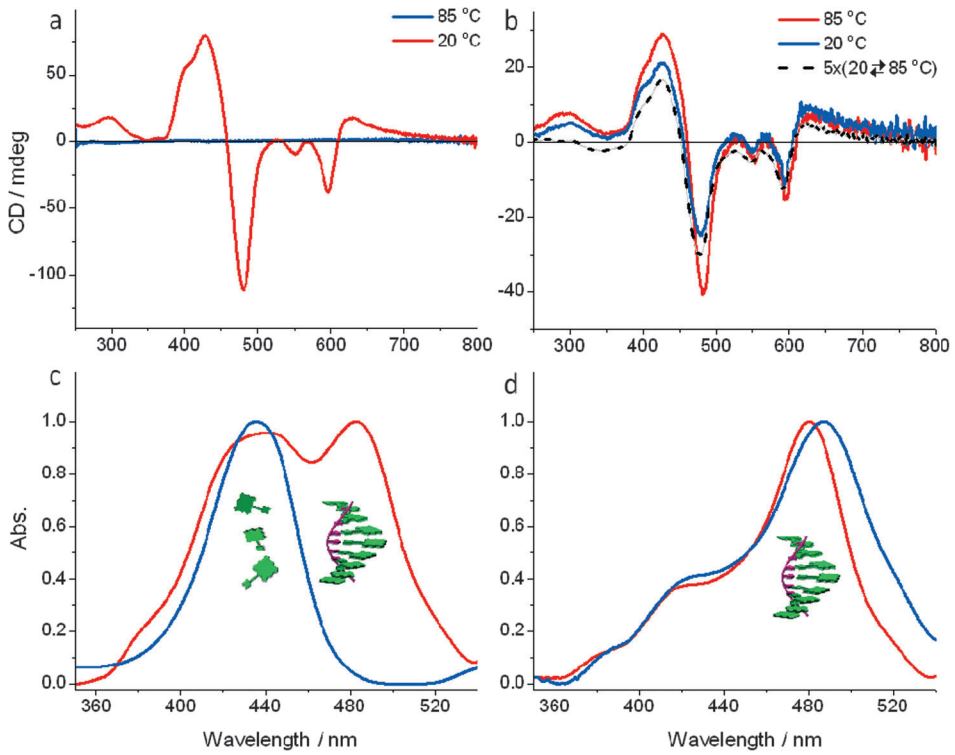

Figure 9. Variable-temperature a), b) CD and c), d) normalized UV/Vis absorption spectra of the right-handed NiPor-DAP:dT40 nanoassembly before dialysis (left spectra) and after dialysis (right spectra) at 20 °C (red), 85 °C (blue), and after five heating–cooling cycles (dashed curve). Assembly formation: [NiPor-DAP] = [dT40] = 10 μM; slow annealing in 45% DMSO, Na-cacodylate buffer (1 mM, pH 7.0, 100 mM NaCl).

thermal stability and analogous spectroscopic behavior upon heating. The intensity of the Soret CD bands decreased; however, the overall CD profile did not change when NiPor-DAP:dT40 nanoassembly was heated from 20 °C to 85 °C (Figure 9b). The UV/Vis absorption experienced a red-shift of the λ_{max} from 480.2 nm to 487.5 nm. Importantly, NiPor-DAP:dT40 remained a chiral right-handed supramolecular structure with even after five heating–cooling cycles. On the other hand, heating the non-dialyzed NiPor-DAP:dT40 from 20 °C to 85 °C caused complete melting, which is evident by the disappearance of the CD signal (Figure 9a). The Soret band showed a small blue-shift (7.1 nm) to 437.9 nm. Sigmoidal fit of the CD signal change at 436.0 nm as a function of temperature allowed us to calculate the Tm = 56.0 °C.

The dialyzed left-handed 2HPor-DAP:dT40 nanoassemblies displayed larger spectroscopic and structural changes upon heating-cooling. The profile of the CD spectrum of the left-handed 2HPor-DAP:dT40 nanoassembly changed after heating from 20 °C to 85 °C, though the assembly retained its counter-clockwise helical structure (Figure 10b). The CD spectrum at 85 °C exhibited significant similarities with original freshly prepared left-handed 2HPor-DAP:dT40 (Figure 2a) with negative CD band 461.2 nm and positive CD bands at 398.5 nm and 505.0 nm. Absorption spectrum exhibited a red-shift from 481.5 nm to 488.8 nm. The emission spectrum stayed virtually identical upon heating to 85 °C.

Five heating-cooling cycles caused very little change of the CD spectrum of the left-handed 2HPor-DAP:dT40 (Figure 10b, dashed curve). In contrast, the non-dialyzed left-handed 2HPor-DAP:dT40 nanoassembly fully melted upon heating and the CD signal completely disappeared above 70 °C (Figure 10a). Sigmoidal fit of the change of the 462 nm CD signal as a function of temperature yielded the Tm = 50.3 °C. The absorption spectrum showed the disappearance of the 486.2 nm band and a small blue-shift (Δ = 7.1 nm) of the 445.0 nm band. The emission spectrum displayed a new band at 673.2 nm after heating to 85 °C.

The dialyzed left-handed NiPor-DAP:dT40 nanoassembly exhibited temperature induced structural changes as evidenced by the CD spectrum. The CD spectrum at 85 °C displayed positive CD bands at 391.4, 492.8, and 602.4 nm and a negative CD band at 465.9 nm (Figure 11b). The UV/Vis absorption showed a red-shift of the λ_{max} from 472.5 nm to 486.8 nm. The helicity of the left-handed NiPor-DAP:dT40 was preserved after five heating–cooling cycles (Figure 11b, dashed curve). On the other hand, heating of the non-dialyzed left-handed NiPor-DAP:dT40 from 20 °C to 85 °C caused its complete disassembly as evident by the absence of a CD signal and the disappearance of the absorption band at 476.2 nm (Figure 11a,c). T_m was calculated to be 46.9 °C using CD signal at 462 nm. Right-handed nanoassemblies prepared by fast cooling showed annealing-induced structural changes towards thermodynamically most stable structure. The thermal studies determined that all dialyzed nanoassemblies exhibited a high degree of thermal stability.

As right-handed 2HPor-DAP:dT40 nanoassemblies prepared by slow annealing exhibited the highest thermal stability we have explored the effect of pH on their stability. In two separate experiments the pH of the 2HPor-DAP:dT40 solution was decreased to 1.7 using HCl or increased to a pH 12.5 using NaOH while measuring UV/Vis and CD spectra (Figure 12). Increasing the pH to 12.5 did not change the shape of the UV/Vis absorption and CD spectra of 2HPor-DAP:dT40 but decreased their intensity. The UV/Vis Soret band signal at 490.7 nm dropped by 23.5%. Ellipticities at 428.5 nm and at 493.4 nm diminished from +31.6 mdeg to +17.0 mdeg (−46.2%) and from −18.5 mdeg to −8.2 mdeg (−55.6%), respectively. Decreasing the pH of right-handed 2HPor-DAP:dT40 solution from 7 to 6 had no effect on the structure of the assemblies as indicated by identical CD and UV/Vis spectra (Figure 12a–c). Decreasing the pH to 3 caused Soret band

© 2014 Wiley-VCH Verlag GmbH & Co. KGaA, Weinheim

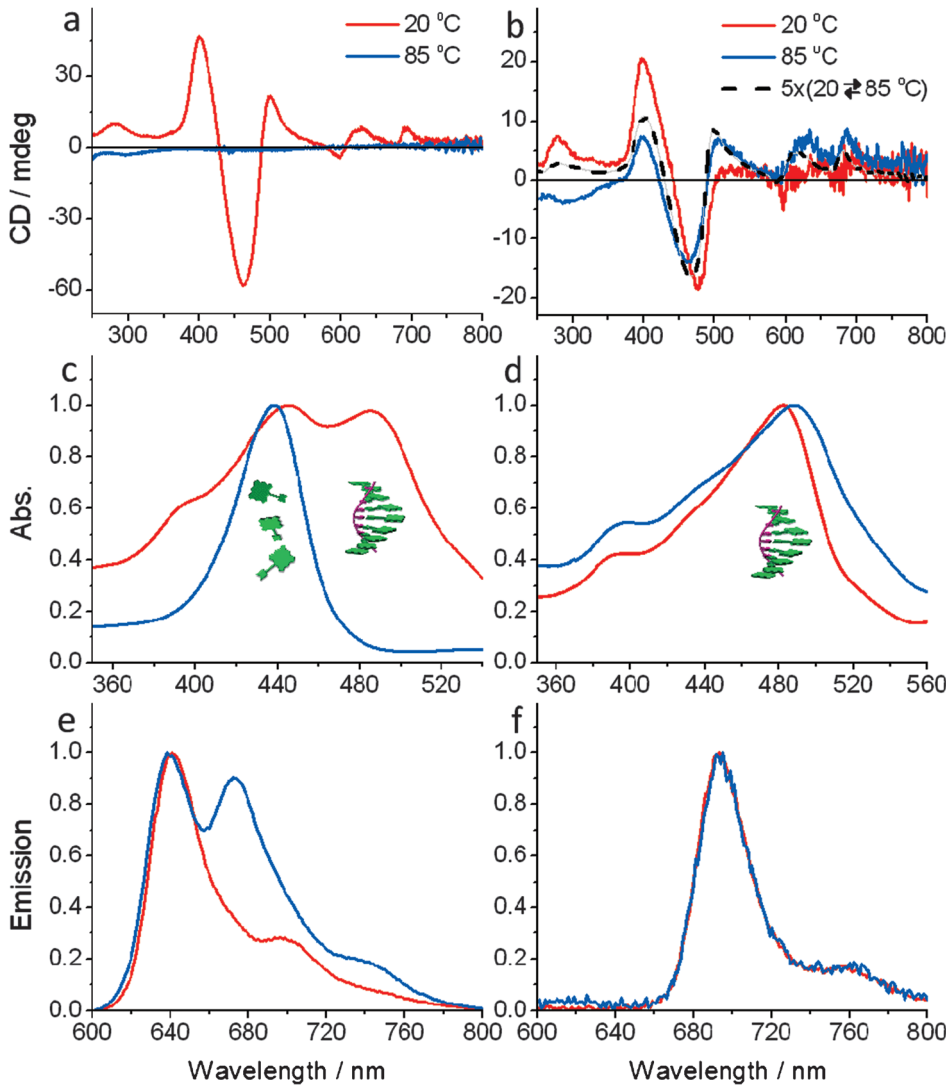

Figure 10. Variable-temperature a), b) CD, normalized c), d) UV/Vis absorption, and e), f) emission spectra of the left-handed 2HPor-DAP:dT40 nanoassembly before dialysis (left spectra) and after dialysis (right spectra) at 20 °C (red), 85 °C (blue), and after five heating–cooling cycles (dashed curve). Assembly formation: [2HPor-DAP] = [dT40] = 10 μM; fast annealing in 40% DMSO Na-cacodylate buffer (1 mM, pH 7.0, 100 mM NaCl).

broadening and 28.7% hypochromicity. CD signal at 428.5 nm dropped to 17.0 mdeg without a wavelength shift. Interestingly, further decrease to pH 1.7 led to increase of the ellipticity together with CD band shifts. The positive Cotton effect shifted from 428.5 nm to 439.5 nm and its intensity increased to 28.5 mdeg. The negative Cotton effect shifted from 493.4 nm to 479.8 nm and its intensity increased to −13.1 mdeg. UV/Vis absorption spectrum showed a blue-shift of the Soret band maximum to 463.0 nm. The absorption peak at 489.0 nm corresponding to original structure of right-handed 2HPor-DAP:dT40 assembly completely disappeared. The right-handed 2HPor-DAP:dT40 nanoassemblies thus possessed excellent acid–base stability with minimal structural changes between pH 3 and 13.

Conclusion

We have shown that free-base and nickel porphyrin–diaminopurine conjugates 2HPor-DAP and NiPor-DAP can be successfully assembled on oligothymidine templates of different lengths into helical supramolecular multiporphyrin nanostructures by hydrogen bonding between complementary thymine and diaminopurine groups. UV/Vis spectroscopy showed strong electronic coupling between porphyrin units, as shown by a strong red-shift of the Soret band (up to 54 nm). The handedness of templated multiporphyrin nanoassemblies could be controlled by the annealing rate and ionic strength during the nanoassembly formation. Slow annealing rates yielded preferentially right-handed nanostructures, whereas fast annealing yielded left-handed nanostructures. The helicities have been assigned with the help of theoretical CD calculations. We have successfully used dialysis to separate porphyrin nanoassemblies from porphyrin monomers. All of the dialyzed DNA-templated porphyrin nanoassemblies had very high values of molar CD (ε of up to $+850\ L\,mol^{-1}\,cm^{-1}$) as well as CD anisotropy (g of up to $+1.0\times10^{-2}$). HRTEM studies confirmed formation of DNA-templated nickel(II)porphyrin nanoassemblies and showed their elongation into helical fibrils with micrometer lengths. The chiral DNA-templated multiporphyrin nanoassemblies exhibited high thermal and pH stability. The handedness of all assemblies was preserved at temperatures up to +85 °C and pH between 3 and 12. We anticipate that chiral DNA-templated porphyrin nanoassemblies will find applications in chiroptical nanomaterials owing to their modular chiroptical and structural properties and high stability.

Experimental Section

All of the commercially available reagents were used as received without purification unless otherwise indicated. Water was obtained from Milli-Q system with a resistivity of 18.2 MΩ cm. DNA concentrations are reported as nucleobase concentration and they were quantified by UV/Vis absorption spectroscopy. All DNA-tem-

© 2014 Wiley-VCH Verlag GmbH & Co. KGaA, Weinheim

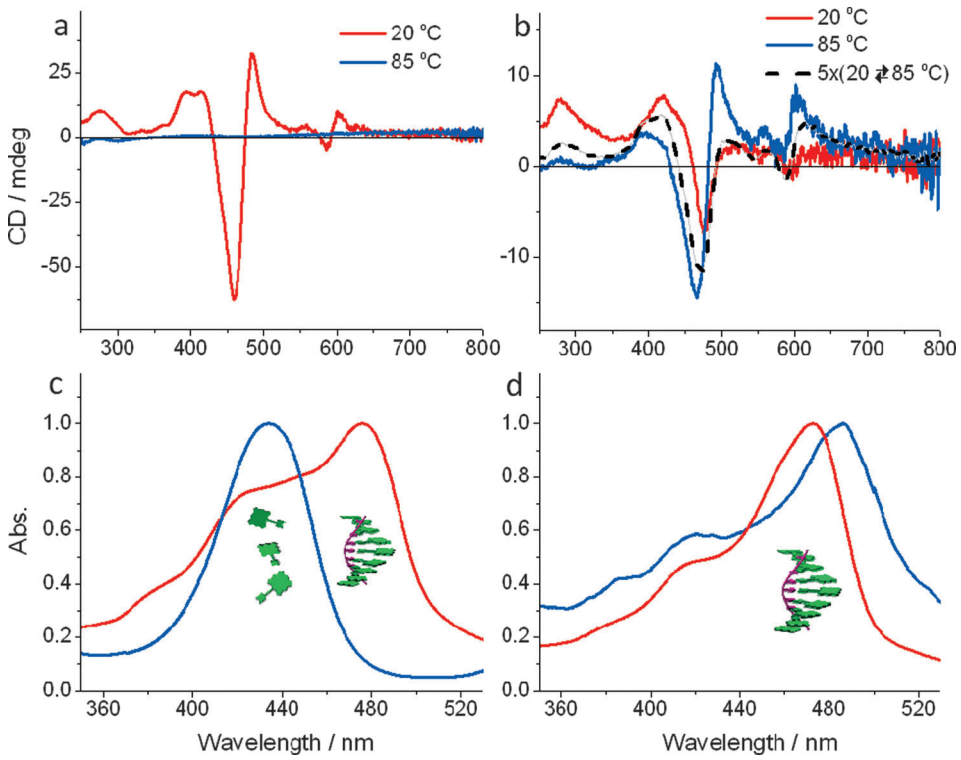

Figure 11. Variable-temperature a),b) CD and c),d) normalized UV/Vis absorption spectra of the left-handed NiPor-DAP:dT40 nanoassembly before dialysis (left spectra) and after dialysis (right spectra) at 20 °C (red curves), 85 °C (blue curves), and after five heating–cooling cycles (dashed curve). Assembly formation: [NiPor-DAP] = [dT40] = 10 μM; fast annealing in 45% DMSO Na-cacodylate buffer (1 mM, pH 7.0, 100 mM NaCl).

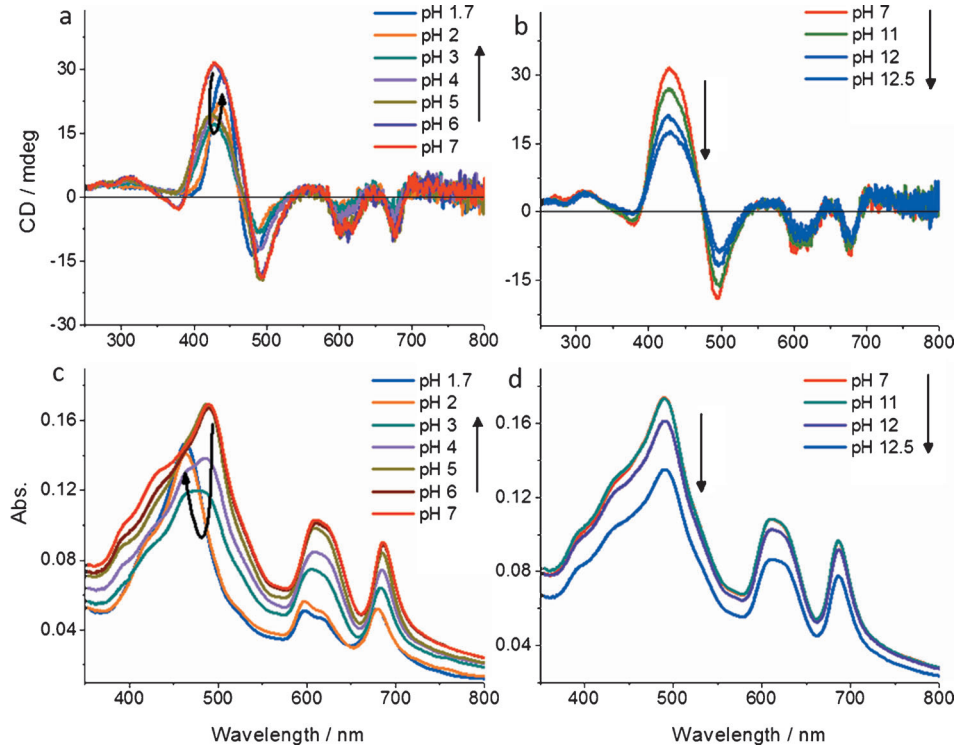

Figure 12. Effect of pH on CD and UV/Vis absorption spectra of right-handed 2HPor-DAP:dT40. Assembly formation: [2HPor-DAP] = [dT40] = 10 μM; slow cooling in 40% DMSO Na-cacodylate buffer (1 mM, pH 7.0, 500 mM NaCl).

plated porphyrin nanoassemblies were prepared following previously reported procedures.[5] CD spectra were recorded on a Jasco J-815 spectropolarimeter equipped with a Peltier temperature control system. Conditions were as follows: scanning speed 50 nm min^{-1}, data pitch 0.5 nm, DIT 2 s, and bandwidth 1 nm. UV/Vis absorption spectra were recorded on a Jasco V-630 double-beam spectrophotometer equipped with a single-position Peltier temperature control system. Fluorescence emission spectra were recorded on the Varian Cary Eclipse fluorescence spectrophotometer equipped with a Peltier temperature-control system. Conditions were as follows: scan rate 600 nm min^{-1}, excitation slit 5.0 nm, and emission slit 5.0 nm. A quartz cuvette with a 1 cm path length was used for all CD, UV/Vis, and emission spectroscopy experiments. ^{1}H NMR spectra were obtained on a Bruker DRX-400 spectrometer (^{1}H: 400 MHz). Chemical shifts are quoted as parts per million (ppm) relative to the solvent residual peak and coupling constants (*J*) are quoted in Hz. A solution of dialyzed NiPor-DAP:dT40 in water was drop-cast onto carbon-coated copper grids and dried in air. Imaging was performed on an FEI Tecnai G2 F20 scanning transmission electron microscope (STEM) operating at 200 kV.

Dialysis

A solution of DNA-templated porphyrin nanoassembly (10 μM, 1.6 mL) in 40% DMSO Na-cacodylate buffer (1 mM, pH 7.0, 100 mM NaCl) was placed into a 2000 Dalton dialysis cassette. The cassette was submerged into the Na-cacodylate buffer (250 mL, 1 mM, pH 7.0) and gently stirred for 12 h. The cassette was then moved to a new buffer solution and stirred for additional 2 h.

9-Methoxy-trietyleneglycol-diaminopurine-2,6 (1)

2,6-diaminopurine (DAP) (500.0 mg, 3.33 mmol) was added to a freshly distilled DMF (15.0 mL) and the resulting suspension was heated to 60 °C under nitrogen

© 2014 Wiley-VCH Verlag GmbH & Co. KGaA, Weinheim

until a solution was formed. NaH (96.0 mg, 4 mmol) was added and the mixture was stirred for 2 h followed by a dropwise addition of triethylene glycol monomethyl ether tosylate (1.059 g, 3.32 mmol) in DMF (5.0 mL) at 0 °C. The reaction was monitored by TLC (CH_2Cl_2/MeOH, 9:1) until no further change was observed (7 h). DMF was evaporated, and the product was purified by flash column chromatography on silica using CH_2Cl_2/MeOH (9:1) as the eluent. Evaporation of the solvent gave (**1**) as a colorless crystalline solid (514.6 mg, 52%). ^{1}H NMR ($CDCl_3$, 400 MHz) $\delta = 3.36$ (s, 3H, O-CH_3), 3.51–3.54 (m, 2H, O-CH_2), 3.57–3.60 (m, 6H, O-CH_2), 3.76 (dd, $J = 5.2$ Hz, 4.8 Hz, 2H, O-CH_2), 4.18 (dd, $J = 5.2$ Hz, 4.8 Hz, 2H, O-CH_2), 4.76 (bs, 2H, NH_2), 5.49 (bs, 2H, NH_2), 7.67 ppm (s, 1H, $H_{8-purine}$); *m/z* ESI $C_{12}H_{20}N_6O_3$ [MH^+] calcd 297.167; found 297.200.

8-Bromo-9-methoxy-trietyleneglycol-diaminopurine-2,6 (2)

TEG-purine **1** (200.0 mg, 0.675 mmol) was added to MeCN (5.0 mL) under nitrogen and the solution was placed in an ice bath. NBS (138 mg, 0.776 mmol) dissolved in MeCN (3.0 mL) was added dropwise over 1 h. The ice bath was removed and the reaction was stirred for 30 min at room temperature. The solvent was evaporated and the product purified by flash column chromatography on silica using CH_2Cl_2/MeOH (97:3) as the eluent. Evaporation of the solvent gave 218.0 mg (87%) of product **2** as a colorless solid. ^{1}H NMR ($CDCl_3$, 400 MHz) $\delta = 3.35$ (s, 3H, O-CH_3), 3.48–3.50 (m, 2H, O-CH_2), 3.54–3.63 (m, 6H, O-CH_2), 3.81 (t, $J = 6.0$ Hz, 2H, O-CH_2), 4.24 (t, $J = 6.0$ Hz, 2H, O-CH_2), 4.78 (bs, 2H, NH_2), 5.36 ppm (bs, 2H, NH_2); *m/z* ESI $C_{12}H_{19}BrN_6O_3$ [MH^+] calcd 375.0783; found 375.0660.

8-Trihexylsilyl-ethynyl-9-methoxy-trietyleneglycol-diaminopurine-2,6 (3)

8-Bromopurine **2** (200.0 mg, 0.534 mmol) was dissolved in piperidine (10.0 mL) and the solution was deoxygenated using a vacuum/nitrogen cycle. Triphenylphosphine (140.0 mg, 0.534 mmol) and [$Pd_2(dba)_3$] (122.2 mg, 0.133 mmol) were added subsequently against positive pressure of nitrogen. Mono(trihexylsilyl)acetylene (492.0 mg, 1.600 mmol) was added to piperidine (3.0 mL) and the solution was deoxygenated using a vacuum/nitrogen cycle. The resulting suspension was deoxygenated, then heated to 40 °C for 10 min. Copper(I) iodide (50.8 mg, 0.267 mmol) was added and reaction was monitored by TLC (CH_2Cl_2/MeOH, 95:5). The starting material disappeared after 4 h. The reaction mixture was cooled to room temperature, the solvent was evaporated, and the product purified by flash column chromatography on silica using ethyl acetate as eluent. Evaporation of the solvent yielded **3** as a white solid (279.0 mg, 87%). ^{1}H NMR ($CDCl_3$, 400 MHz) $\delta =$ 0.70–0.74 (m, 6H, hexyl), 0.88–0.92 (m, 9H, CH_2, hexyl), 1.24–1.45 (m, 24H, hexyl), 3.34 (s, 3H, O-CH_3), 3.46–3.48 (m, 2H, O-CH_2), 3.53–3.62 (m, 6H, O-CH_2), 3.84 (t, $J = 6.0$ Hz, 2H, O-CH_2), 4.29 (t, $J =$ 6.0 Hz, 2H, O-CH_2), 4.81 (bs, 2H, NH_2), 5.39 ppm (bs, 2H, NH_2); *m/z* ESI $C_{32}H_{58}N_6O_3Si$ [MH^+] calcd 603.441; found 603.666.

8-Ethynyl-9-methoxy-trietyleneglycol-diaminopurine-2,6 (4)

THS-diaminourine **3** (108.8 mg, 0.180 mmol) was dissolved in CH_2Cl_2 (5 mL) under nitrogen. TBAF (550.0 μL, 1 M solution in THF, 0.550 mmol) was added. The reaction mixture was stirred at room temperature for 30 min followed by addition of anhydrous granular calcium chloride (ca. 200 mg). The solvent was reduced by evaporation and the reaction mixture passed through a silica gel column using CH_2Cl_2/MeOH (9:1) as eluent. Evaporation of the solvent gave 52.0 mg (90%) of diaminopurine **4** as a white solid. ^{1}H NMR ($CDCl_3$, 400 MHz) $\delta = 3.35$ (s, 3H, O-CH_3), 3.41 (s, 1H, acetylene), 3.48–3.50 (m, 2H, O-CH_2), 3.55–3.63 (m, 6H, O-CH_2), 3.84 (t, $J = 6.0$ Hz, 2H, O-CH_2), 4.31 (t, $J = 6.0$ Hz, 2H, O-CH_2), 4.82 (bs, 2H, NH_2), 5.48 ppm (bs, 2H, NH_2); *m/z* ESI $C_{14}H_{20}N_6O_3$ [MH^+] calcd 321.167; found 321.133.

5,15-Diaryl-porphyrin (6)

Dipyrromethane (1.80 g, 12.36 mmol) and 3,4-bis-substituted aldehyde **5** (5.32 g, 12.36 mmol) were dissolved in CH_2Cl_2 (2.4 L) under nitrogen. TFA (600 μL) was added to the resulting solution by a syringe. The flask was shielded from light with aluminum foil and the solution stirred at room temperature for 3 h. 2,3-Dichloro-5,6-dicyano-1,4-benzoquinone (DDQ; 3.60 g, 15.80 mmol) was added and the solution stirred for additional 30 min. The mixture was neutralized with triethylamine (TEA, 12.0 mL, 0.086 mol) and poured directly onto a silica gel pad (4 cm x 7 cm). Fast-running DDQ residues were removed by CH_2Cl_2 and the product eluted with CH_2Cl_2/MeOH (95:5). The product was further purified by a flash silica gel column chromatography using CH_2Cl_2/MeOH (98:2) as the eluent. On removal of solvent and drying under high vacuum, product **6** (3.40 g, 49%) was obtained as purple solid glass. ^{1}H NMR ($CDCl_3$, 400 MHz) $\delta = -3.07$ (br. s, 2H, N-H pyrrole), 3.21 (s, 6H, O-CH_3), 3.33 (t, $J = 12.0$ Hz, 4H), 3.42 (bs, 6H, O-CH_3), 3.49 (dd, $J = 5.0$ Hz, 4 Hz, 4H), 3.64–3.70 (m, 8H), 3.77–3.84 (m, 8H), 3.80 (m, 4H), 3.90–3.96 (m, 8H), 4.10 (m, 4H), 4.35–4.42 (m, 4H), 4.50 (m, 4H), 7.29 (d, $J = 8.0$ Hz, 2H, Ar), 7.40 (d, $J = 8.0$ Hz, 2H, Ar), 7.78 (s, 2H, Ar), 9.09 (d, $J = 4.0$ Hz, 4H, β-H), 9.35 (d, $J = 4.0$ Hz, 4H, β-H), 10.23 ppm (s, 2H, *meso*-H); *m/z* ESI $C_{60}H_{78}N_4O_{16}$ [MH^+] calcd 1111.55; found 1111.80.

5,15-Diaryl-Zn-porphyrin (7)

A solution of zinc acetate dihydrate (5.96 g, 27.18 mmol) in MeOH (50 μL) was added to a stirred solution of porphyrin **6** (3.40 g, 3.02 mmol) in a 1:1 mixture of CH_2Cl_2/MeOH (100 μL). The reaction mixture was stirred for another 45 min, after which TLC (CH_2Cl_2/MeOH, 95:5) confirmed completion. Evaporation of the solvent and flash chromatography on silica, eluted with CH_2Cl_2/MeOH (95:5), was carried out to remove the excess zinc salts. Evaporation of the solvent gave zinc porphyrin **7** as a red glass (2.81 g, 78%). ^{1}H NMR ($CDCl_3$, 400 MHz) $\delta = 3.21$ (s, 6H, O-CH_3), 3.33 (m, 4H), 3.42 (s, 6H, O-CH_3), 3.49 (m, 4H), 3.64 (m, 8H), 3.75 (m, 8H), 3.80 (m, 4H), 3.90–3.96 (m, 8H), 4.09 (m, 4H), 4.35 (m, 4H), 4.50 (m, 4H), 7.23 (d, $J =$ 8.0 Hz, 2H, Ar), 7.79 (dd, $J = 8.0$ Hz, 2 Hz, 2H, Ar), 7.92 (dd, $J =$ 8.0 Hz, 2.0 Hz, 2H, Ar), 9.14 (d, $J = 2.0$ Hz, 2H, β-H), 9.15 (d, $J =$ 2.0 Hz, 2H, β-H), 9.38 (d, $J = 2.0$ Hz, 2H, β-H), 6.39 (d, $J = 2.0$ Hz, 2H, β-H), 10.24 ppm (d, $J = 2.0$ Hz, 2H, *meso*-H); *m/z* ESI $C_{60}H_{76}N_4O_{16}Zn$ [MH^+] calcd 1173.46; found 1173.70.

Monobrominated Zn-porphyrin (8)

Zinc porphyrin **7** (1.90 g, 1.62 mmol) was dissolved in chloroform (200 mL) with pyridine (375 μL). A solution of NBS (288 mg, 1.62 mmol) in chloroform (40 mL) and pyridine (190 μL) was added dropwise over 60 min. The reaction was stirred for 15 min and then quenched with acetone (5 mL). The solvents were removed under reduced pressure, and the product **8** was purified by flash silica chromatography using 50:35:15 Hexane/Toluene/MeOH. Evaporation of the solvents gave monobrominated zinc porphyrin **8** (547 mg, 27%). ^{1}H NMR ($CDCl_3$/1% C_5D_5N, 400 MHz) $\delta = 3.21$ (s, 6H, O-CH_3), 3.33–3.35 (m, 4H), 3.41 (s, 6H, O-CH_3), 3.48–3.50 (m, 4H), 3.59–3.62 (8H, m, $J = 9$ Hz, 4.5 Hz), 3.72–3.80 (m, 12H), 3.88–3.94 (m, 8H), 4.07 (t, $J = 4.5$ Hz, 4H), 4.33 (t, $J = 4.5$ Hz, 4H), 4.48 (t, $J = 4.5$ Hz, 4H), 7.27 (d, $J =$ 8.0 Hz, 2H, Ar), 7.68 (d, $J = 8.0$ Hz, 2H,

© 2014 Wiley-VCH Verlag GmbH & Co. KGaA, Weinheim

Ar), 7.79 (s, 2H, Ar), 8.97–8.99 (m, $J=4.0$ Hz, 4H, β-H), 9.25 (d, $J=4.5$ Hz, 2H, β-H), 9.71 (d, $J=4.5$ Hz, 2H, β-H), 10.06 ppm (s, 1H, *meso*-H); *m/z* ESI $C_{60}H_{75}N_4O_{16}Zn$ $[M\text{-Na}]^+$ calcd 1273.36; found 1273.54.

ZnPor-DAP

The monobrominated Zn-porphyrin **8** (360.0 mg, 0.287 mmol) was dissolved in freshly distilled DMF (10.0 mL) under nitrogen followed by addition of TEA (8.0 mL). The solution was deoxygenated (vacuum/nitrogen cycle) and triphenylphosphine (75.2 mg, 0.287 mmol) and $[Pd_2(dba)_3]$ (65.0 mg, 0.071 mmol) were added subsequently. Next, acetylene–diaminopurine **4** (165.1 mg, 0.515 mmol) was added in DMF (5.0 mL). The resulting mixture was deoxygenated (vacuum/nitrogen cycle), then heated to 40 °C for 10 min. Copper(I) iodide (27.3 mg, 0.143 mmol) was added and reaction was stirred at 40 °C overnight (15 h) when TLC (CH_2Cl_2/MeOH, 95:5) confirmed completion. The mixture was cooled and the solvents removed. Porphyrin–diaminopurine ZnPor-DAP was obtained as a green glass (290.0 mg, 67%) by flash silica chromatography using CH_2Cl_2/MeOH/pyridine (90:9:1). ^{1}H NMR ($CDCl_3$, 400 MHz) $\delta=3.07$ (s, 3H, O-CH_3), 3.16 (dd, $J=4.6$ Hz, 4.4 Hz, 2H), 3.21 (s, 6H, O-CH_3), 3.34–3.40 (m, 6H), 3.41 (s, 6H, O-CH_3), 3.49–3.52 (m, 4H), 3.58–3.63 (m, 10H), 3.73–3.81 (m, 14H), 3.90–3.96 (m, 8H), 4.09 (t, $J=5.0$ Hz, 4H), 4.21 (t, $J=5.0$ Hz, 2H), 4.34 (t, $J=8.0$ Hz, 4H), 4.49 (t, $J=8.0$ Hz, 4H), 4.82 (t, $J=5.5$ Hz, 2H), 4.86 (bs, 2H, NH_2), 5.59 (bs, 2H, NH_2), 7.27 (d, $J=8.0$ Hz, 2H, Ar), 7.68 (dd, $J=8.0$ Hz, 2.0 Hz, 2H, Ar), 7.80 (d, $J=2.0$ Hz, 2H, Ar), 8.95 (d, $J=4.5$ Hz, 2H, β-H), 9.00 (d, $J=4.5$ Hz, 2H, β-H), 9.25 (d, $J=4.5$ Hz, 2H, β-H), 9.79 (d, $J=4.5$ Hz, 2H, β-H), 10.11 ppm (s, 1H, *meso*-H); MALDI/TOF: *m/z* $C_{74}H_{94}N_{10}O_{19}Zn$ $[M\text{-H}^+]$ calcd 1491.6066; found 1491.6025. UV/Vis λ_{max} (DMSO) (log ε) = 451.8 nm (5.33), 576.4 nm (4.18), 636.0 nm (4.62).

2HPor-DAP

Zn^{II} porphyrin–diaminopurine (15.0 mg, 0.010 mmol) was dissolved in CH_2Cl_2 (2.5 mL). The solution was stirred in a flask in an ice bath for 15 min, and then TFA (100 μL) was added dropwise. After 10 min the ice bath was removed and the reaction was stirred at room temperature for 4 h. Then the flask was placed in an ice bath and a saturated solution of $NaHCO_3$ (20.0 mL) was added. The ice bath was removed and solution was stirred at room temperature for 30 min. The mixture was extracted with CH_2Cl_2 (3×20 mL) and combined organic layers washed with water (20 mL). The CH_2Cl_2 was evaporated and the product was purified by flash column chromatography on silica using CH_2Cl_2/MeOH (9:1) as the eluent. 2HPor-DAP was obtained as a green glass (10 mg, 70%). ^{1}H NMR ($CDCl_3$, 400 MHz) $\delta=-2.52$ (s, 2H, pyrrole), 3.03 (s, 3H, O-CH_3), 3.12–3.15 (m, 2H), 3.19 (s, 3H, O-CH_3), 3.20 (s, 3H, O-CH_3), 3.31–3.38 (m, 6H), 3.42 (s, 6H, O-CH_3), 3.49–3.52 (m, 4H), 3.58–3–64 (m, 10H), 3.74–3.81 (m, 14H), 3.91–3.97 (m, 8H), 4.09–4.11 (m, 4H), 4.19 (t, $J=5.0$ Hz, 2H,), 4.32–4.35 (m, 4H), 4.49–4.51 (m, 4H), 4.80 (t, $J=5.5$ Hz, 2H), 4.85 (bs, 2H, NH_2), 5.53 (bs, 2H, NH_2), 7.32 (d, $J=8.0$ Hz, 2H, Ar), 7.74 (dd, $J=8.0$ Hz, 2.0 Hz, 2H, Ar), 7.82 (d, $J=2.0$ Hz, 2H, Ar), 8.97 (d, $J=4.5$ Hz, 2H, β-H), 9.02 (d, $J=4.5$ Hz, 2H, β-H), 9.27 (d, $J=4.5$ Hz, 2H, β-H), 9.84 (d, $J=4.5$ Hz, 2H, β-H), 10.19 ppm (s, 1H, *meso*-H); HR-ESI: $C_{74}H_{96}N_{10}O_{19}$, *m/z* $[M\text{-H}^+]$ calcd 1429.6931; found 1429.6920. UV/Vis: λ_{max} (DMSO) (log ε) = 437.0 nm (5.18), 592.0 nm (4.44), 673.0 nm (4.15).

NiPor-DAP

The free-base porphyrin–diaminopurine (2HPor-DAP) (11.0 mg, 0.0076 mmol) was dissolved in freshly distilled DMF (3.0 mL) under nitrogen followed by addition of nickel(II) acetate tetrahydrate (19.1 mg). The solution was heated to 120 °C for 4 h when TLC (CH_2Cl_2/MeOH, 95:5) showed completion. DMF was evaporated under reduced pressure and the residue was dissolved in CH_2Cl_2 (20 mL) and washed with water (10 mL). NiPor-DAP was purified by flash silica gel chromatography with $CHCl_3$/MeOH/TEA (90:9:1). Yield 9.6 mg, 83%. ^{1}H NMR ($CDCl_3$, 400 MHz) $\delta=3.04$ (s, 3H, O-CH_3), 3.11–3.13 (m, 2H), 3.21 (s, 6H, O-CH_3), 3.26–3.36 (m, 6H), 3.41 (s, 6H, O-CH_3), 3.48–3.50 (m, 4H), 3.53–3.55 (m, 2H), 3.59–3.62 (m, 8H), 3.68–3.76 (m, 14H), 3.87–3.92 (m, 8H), 4.05 (dd, $J=5.5$ Hz, 5.0 Hz, 4H), 4.12 (t, $J=5.5$ Hz, 2H), 4.27–4.29 (m, 4H), 4.45 (m, 4H), 4.71 (t, $J=5.5$ Hz, 2H), 4.84 (bs, 2H, NH_2), 5.53 (bs, 2H, NH_2), 7.24 (d, $J=8.0$ Hz, 2H, Ar), 7.55 (dd, $J=8.0$ Hz, 2.0 Hz, 2H, Ar), 7.61 (d, $J=2.0$ Hz, 2H, Ar), 8.90 (d, $J=4.5$ Hz, 2H, β-H), 8.94 (d, $J=4.5$ Hz, 2H, β-H), 9.11 (d, $J=4.5$ Hz, 2H, β-H), 9.71 (d, $J=4.5$ Hz, 2H, β-H), 9.76 ppm (s, 1H, *meso*-H); Triethylamine coordinated on Ni: $\delta=$ 1,20 (t, $J=7.0$ Hz, 9H, CH_3), 3.47 ppm (q, $J=7.0$ Hz, 6H, CH_2). Coordination of solvents (for example DMF, MeOH, water) to metal center porphyrins has been previously reported in magnesium porphyrins.[13] MALDI/TOF: *m/z* $C_{74}H_{94}N_{10}NiO_{19}$ $[M-H^+]$ calcd 1485.6128; found 1485.6212. UV/Vis λ_{max} (DMSO) (log ε) = 436.6 nm (5.05), 544.4 nm (4.25), 591.2 nm (4.37).

Acknowledgements

This work was supported by the UW Start-up Funds (M.B.), University of Wyoming, School of Energy Resources Graduate Assistantship (M.B., G.S.), SER Center for Photoconversion and Catalysis (M.B., G.S.), and NSF Career 0846140 (J.K.).

Keywords: circular dichroism · porphyrins · self-assembly · supramolecular chemistry · TDDFT calculations

[1] a) R. Purrello, *Nat. Mater.* **2003**, *2*, 216–217; b) L. Rosaria, A. D'Urso, A. Mammana, R. Purrello, *Chirality* **2008**, *20*, 411–419; c) T. Nakashima, Y. Kobayashi, T. Kawai, *J. Am. Chem. Soc.* **2009**, *131*, 10342–10343; d) H. Onouchi, T. Miyagawa, K. Morino, E. Yashima, *Angew. Chem.* **2006**, *118*, 2441–2444; *Angew. Chem. Int. Ed.* **2006**, *45*, 2381–2384; e) A. J. Gellman, *ACS Nano* **2010**, *4*, 5–10; f) C. Gautier, T. Bürgi in *Chiral Nanoparticles, Vol.* Wiley-VCH, Weinheim, **2009**, pp. 67–91; g) U. Tohgha, K. Varga, M. Balaz, *Chem. Commun.* **2013**, *49*, 1844–1846; h) Y. Li, M. Wang, T. J. White, T. J. Bunning, Q. Li, *Angew. Chem.* **2013**, *125*, 9093–9097; *Angew. Chem. Int. Ed.* **2013**, *52*, 8925–8929; i) R. Pfukwa, P. H. J. Kouwer, A. E. Rowan, B. Klumperman, *Angew. Chem.* **2013**, *125*, 11246–11250; *Angew. Chem. Int. Ed.* **2013**, *52*, 11040–11044; j) U. Tohgha, K. K. Deol, A. G. Porter, S. G. Bartko, J. K. Choi, B. M. Leonard, K. Varga, J. Kubelka, G. Muller, M. Balaz, *ACS Nano* **2013**, *7*, 11094–11102.

[2] a) M. Jurow, A. E. Schuckman, J. D. Batteas, C. M. Drain, *Coord. Chem. Rev.* **2010**, *254*, 2297–2310; b) C. M. Drain, A. Varotto, I. Radivojevic, *Chem. Rev.* **2009**, *109*, 1630–1658; c) T. Nguyen, A. Brewer, E. Stulz, *Angew. Chem.* **2009**, *121*, 2008–2011; *Angew. Chem. Int. Ed.* **2009**, *48*, 1974–1977; d) G. Sargsyan, M. Balaz, *Org. Biomol. Chem.* **2012**, *10*, 5533–5540; e) M. Balaz, B. C. Li, G. A. Ellestad, N. Berova, *Angew. Chem.* **2006**, *118*, 3610–3613; *Angew. Chem. Int. Ed.* **2006**, *45*, 3530–3533; f) F. J. M. Hoeben, M. Wolffs, J. Zhang, S. DeFeyter, P. Leclere, A. P. H. J. Schenning, E. W. Meijer, *J. Am. Chem. Soc.* **2007**, *129*, 9819–9828; g) F. D'Souza, L. M. Rogers, D. M. S. Islam, Y. Araki, O. Ito, *Chem. Lett.* **2008**, *37*, 460–461.

© 2014 Wiley-VCH Verlag GmbH & Co. KGaA, Weinheim

[3] a) J. M. Ribó, J. Crusats, F. Sagués, J. Claret, R. Rubires, *Science* **2001**, *292*, 2063 – 2066; b) A. D'Urso, R. Randazzo, L. Lo Faro, R. Purrello, *Angew. Chem.* **2010**, *122*, 112 – 116; *Angew. Chem. Int. Ed.* **2010**, *49*, 108 – 112.

[4] N. Micali, H. Engelkamp, P. G. van Rhee, P. C. M. Christianen, L. M. Scolaro, J. C. Maan, *Nat. Chem.* **2012**, *4*, 201 – 207.

[5] G. Sargsyan, A. A. Schatz, J. Kubelka, M. Balaz, *Chem. Commun.* **2013**, *49*, 1020 – 1022.

[6] a) P. G. A. Janssen, J. Vandenbergh, J. L. J. van Dongen, E. W. Meijer, A. Schenning, *J. Am. Chem. Soc.* **2007**, *129*, 6078 – 6079; b) P. G. A. Janssen, A. Ruiz-Carretero, D. González-Rodríguez, E. W. Meijer, A. P. H. J. Schenning, *Angew. Chem.* **2009**, *121*, 8247 – 8250; *Angew. Chem. Int. Ed.* **2009**, *48*, 8103 – 8106; c) S. Sezi, H.-A. Wagenknecht, *Chem. Commun.* **2013**, *49*, 9257 – 9259; d) T. J. Bandy, A. Brewer, J. R. Burns, G. Marth, T. Nguyen, E. Stulz, *Chem. Soc. Rev.* **2011**, *40*, 138 – 148; e) M. Fathalla, C. M. Lawrence, N. Zhang, J. L. Sessler, J. Jayawickramarajah, *Chem. Soc. Rev.* **2009**, *38*, 1608 – 1620; f) M. Surin, P. G. A. Janssen, R. Lazzaroni, P. Leclère, E. W. Meijer, A. P. H. J. Schenning, *Adv. Mater.* **2009**, *21*, 1126 – 1130; g) P. G. A. Janssen, S. Jabbari-Farouji, M. Surin, X. Vila, J. C. Gielen, T. F. A. de Greef, M. R. J. Vos, P. H. H. Bomans, N. A. J. M. Sommerdijk, P. C. M. Christianen, P. Lecle're, R. Lazzaroni, P. van der Schoot, E. W. Meijer, A. P. H. J. Schenning, *J. Am. Chem. Soc.* **2009**, *131*, 1222 – 1231; h) W. Yang, P. F. Xia, M. S. Wong, *Org. Lett.* **2010**, *12*, 4018 – 4021; i) W. Yang, Y. Chen, M. S. Wong, P. K. Lo, *Biomacromolecules* **2012**, *13*, 3370 – 3376.

[7] a) A. Ruiz-Carretero, P. G. A. Janssen, A. Kaeser, A. P. H. J. Schenning, *Chem. Commun.* **2011**, *47*, 4340 – 4347; b) A. A. Bruce in *DNA-Templated Assembly of Helical Multichromophore Aggregates, Vol.*, CRC, **2005**, pp. 255 – 287; c) G. Sargsyan, B. L. MacLeod, U. Tohgha, M. Balaz, *Tetrahedron* **2012**, *68*, 2093 – 2099.

[8] a) D. R. McMillin, A. H. Shelton, S. A. Bejune, P. E. Fanwick, R. K. Wall, *Coord. Chem. Rev.* **2005**, *249*, 1451 – 1459; b) J. K. Choi, A. D'Urso, M. Balaz, *J. Inorg. Biochem.* **2013**, *127*, 1 – 6.

[9] J. Brunner, R. Kraemer, *J. Am. Chem. Soc.* **2004**, *126*, 13626 – 13627.

[10] J. K. Choi, G. Sargsyan, M. Shabbir-Hussain, A. E. Holmes, M. Balaz, *J. Phys. Chem. B* **2011**, *115*, 10182 – 10188.

[11] A. Mammana, G. Pescitelli, T. Asakawa, S. Jockusch, A. G. Petrovic, R. R. Monaco, R. Purrello, N. J. Turro, K. Nakanishi, G. A. Ellestad, M. Balaz, N. Berova, *Chem. Eur. J.* **2009**, *15*, 11853 – 11866.

[12] *Gaussian 09*, *Vol.* M. J. Frisch, G. W. Trucks, H. B. Schlegel, G. E. Scuseria, M. A. Robb, J. R. Cheeseman, G. Scalmani, V. Barone, B. Mennucci, G. A. Petersson, H. Nakatsuji, M. L. Caricato, X. Li, H. P. Hratchian, A. F. Izmaylov, J. Bloino, G. Zheng, J. L. Sonnenberg, M. Hada, M. Ehara, K. Toyota, R. Fukuda, J. Hasegawa, M. Ishida, T. Nakajima, Y. Honda, O. Kitao, H. Nakai, T. Vreven, J. A. Montgomery, Jr., J. E. Peralta, F. Oliaro, M. Bearpark, J. J. Heyd, E. Brothers, K. N. Kudin, V. N. Staroverov, R. Kobayashi, J. Normand, K. Raghavachari, A. Rendell, J. C. Burant, S. S. Iyengar, J. Tomasi, M. Cossi, N. Rega, N. J. Millam, M. Klene, J. E. Knox, J. B. Cross, V. Bakken, C. Adamo, J. Jaramillo, R. Gomperts, R. E. Stratmann, O. Yazyev, A. J. Austin, R. Cammi, C. Pomelli, J. W. Ochterski, R. L. Martin, K. Morokuma, V. G. Zakrzewski, G. A. Voth, P. Salvador, J. J. Dannenberg, S. Dapprich, A. D. Daniels, Ö. Farkas, J. B. Foresman, J. V. Ortiz, J. Cioslowski, D. J. Fox, Gaussian, Inc., Wallingford CT, **2009**.

[13] J. S. Lindsey, J. N. Woodford, *Inorg. Chem.* **1995**, *34*, 1063 – 1069.

Received: October 24, 2013
Published online on January 23, 2014

© 2014 Wiley-VCH Verlag GmbH & Co. KGaA, Weinheim